Rare Metal Materials and Engineering
Volume 55, Issue 9, September 2026
Available online at www.rmme.ac.cn

Science Press

Cite this article as: Xu Zhou, Cui Jiayin, He Chang, et al. High-Entropy Metallic Glasses: A Review of Recent Research Progress[J]. Rare Metal Materials and Engineering, 2026, 55(09): 2238-2256. DOI: https://doi.org/10.12442/j.issn.1002-185X.20260028.

REVIEW

High-Entropy Metallic Glasses: A Review of Recent Research Progress

Xu Zhou, Cui Jiayin, He Chang, Gu Jingda, Wang Qing

State Key Laboratory of Materials for Advanced Nuclear Energy, School of Materials Science and Engineering, Shanghai University, Shanghai 200444, China

Abstract: Over the past years, high-entropy metallic glasses (HEMGs) have attracted increasing research interest due to their unique structural characteristics arising from high configurational entropy, as well as distinctive properties such as sluggish diffusion, microstructural heterogeneity, enhanced glass-forming ability (GFA), and improved thermal/mechanical stability. Similar to conventional metallic glasses (MGs), HEMGs lack long-range atomic periodicity; however, the high-entropy effect introduces additional complexity in structural evolution, such as decoupling of the glass transition, potential glass-to-glass transitions, and a continuous polyamorphic transition during reheating. This enables HEMGs with tunable atomic rearrangement, atomic interactions, and chemical/topological heterogeneity, thereby conferring great potential for achieving superior structural and functional properties. Although several review papers have summarized the development of HEMGs, the rapid advancement of this field inspires us to provide a concise overview discussion of the latest research progress in HEMG-forming alloy systems. This review first focused on the GFA of newly developed HEMGs, followed by a comparative analysis of their unusual structural relaxation, crystallization behavior, and mechanical properties relative to conventional MGs. Finally, the unique atomic-scale structure and structural heterogeneity of HEMGs were reviewed, and the review concluded with a summary and outlook.

Key words: high-entropy metallic glasses; glass-forming ability; thermal stability; mechanical property; atomic-scale structure

1 Introduction

High-entropy alloys (HEAs) are a new class of materials composed of multiple principal elements (typically 4 – 6 or more) in near-equiatomic ratios, with each element content accounting for 5at% – 35at%[1–3]. The maximized configurational entropy (typically $\Delta S_{mix} \geqslant 1.5R$, where R is the gas constant[4–5]) in multi-principal element alloy systems generally leads to four core effects: high-entropy stabilization, sluggish diffusion, lattice distortion, and the cocktail effect (synergistic property enhancement)[6–14]. Metallic glasses (MGs) are advanced amorphous metals characterized by a disordered atomic structure lacking long-range periodicity, typically formed by rapid quenching from the melt to prevent crystallization. Because of the amorphous atomic structure, conventional MGs, usually composed of one or two principal elements with minor additions, exhibit superb physical and mechanical properties[15–19]. Intriguingly, as HEAs have rapidly developed, the combination of compositional complexity with the amorphous structure of conventional MGs has led to the discovery of high-entropy metallic glasses (HEMGs), an amorphous subclass of HEAs. HEMGs incorporate multiple principal elements in near-equiatomic proportions, utilizing high configurational entropy to stabilize the glassy phase. As a result, the high-entropy effect endows HEMGs with superior properties exceeding those of traditional MGs or HEAs in certain aspects, including enhanced thermal stability[20–23], sluggish diffusion[24], slow crystallization kinetics[25–28], high mechanical strength[29–34], and, in some cases, excellent magnetic or biomedical performance.

Research on HEMGs has advanced rapidly in recent years, building on the foundations of HEAs (pioneered around

Received date: January 20, 2026
Foundation item: National Natural Science Foundation of China (52171161, U23A2065); Project of Space Utilization System of China Manned Space Engineering (KJZ-YY-NCL08)
Corresponding author: Wang Qing, Ph. D., Associate Professor, State Key Laboratory of Materials for Advanced Nuclear Energy, School of Materials Science and Engineering, Shanghai University, Shanghai 200444, P. R. China, E-mail: qingwang@shu.edu.cn

2004[35]) and MGs (dating back to the 1960s[36]). Since the first report of HEMG in 2011, over 100 distinct HEMG components have been developed[37], which can be categorized into groups such as Ti-Zr-based[26,38–41], Fe-Co-Ni-based[21,42–45], rare-earth-based systems[46–49], and others, mostly derived from conventional MGs by adjusting composition to increase entropy. This growth reflects the increasing interest in leveraging entropy effects to enhance the properties of MG material. This study briefly reviewed the latest advances in HEMG-forming alloy systems and their glass-forming ability (GFA). Then, it focused on the unusual structural relaxation and glass-transition behavior of HEMGs compared with those of conventional MGs[50–60]. Finally, the distinct crystallization behavior and thermal stability of HEMGs were summarized and discussed in terms of their unique dynamic structural evolution.

2 Formation and Formation Criteria of HEMGs

Since the discovery of Au-Si MG in the 1960s[36], great efforts have been devoted to exploring MG-forming alloy systems[54,57,59–60] and fundamentally understanding their GFA from the viewpoint of thermodynamics[61], kinetics[62], and atomic-scale structure[63–64]. Early MG-forming alloy systems such as Au-Si and Pd-Si require extremely high cooling rates (around 106 K/s) to avoid crystallization, thereby restricting their formation into thin films or ribbons[60,65–66]. A significant milestone came in the 1990s with the development of multicomponent alloys with enhanced GFA, such as La-Al-Ni, Zr-based, and Pd-based systems, enabling the synthesis of bulk MGs[67–68]. According to the MG literature[66,69], the development of these high-GFA MGs basically follows the “confusion principle” proposed by Greer[70] and empirical rules later proposed by Inoue et al[71]. The “confusion principle”[70] proposes that multicomponent systems (i. e., more elements) reduce the likelihood of forming stable crystal structures, thereby favoring amorphization in MG-forming alloys. Inoue’s rules[71] state that favorable MG-forming systems, in which atomic mismatch is promoted to restrict long-range diffusion, suppressing crystallization, satisfy three conditions: (1) at least three constituent elements; (2) atomic size differences (δ) ⩾12%; (3) large negative mixing enthalpy (ΔH_{mix}). In principle, a large atomic size difference disrupts lattice formation and promotes amorphous packing, while negative ΔH_{mix} enhances atomic bonding in the amorphous state.

In the 2000s, the principles of HEAs[7–8], which typically incorporate multiple principal elements (often 4–6 or more) in near-equiatomic ratios, were combined with MG formation to develop novel MG-forming alloy systems. The first HEMG, $Ti_{20}Zr_{20}Hf_{20}Ni_{20}Cu_{20}$, was reported in 2002[72], followed by systems such as $Pd_{20}Pt_{20}Cu_{20}Ni_{20}P_{20}$, which broadened the applications of MGs to implants, catalysts, and microelectro-mechanical systems[15]. Since then, HEMGs have garnered increasing attention in materials science and condensed matter physics[73–77].

To date, about 100 HEMGs have been successfully developed and can be broadly categorized into Zr-Ti-, Pd-Pt-, Fe-Co-Ni-, and rare-earth-based systems, as listed in Table S1. The table also lists their thermal characteristic parameters (such as onset temperature of crystallization T_x, glass transition temperature T_g, liquidus temperature T_l, δ, ΔH_{mix}, and ΔS_{mix}) and GFA metrics (such as critical casting thickness D_c, reduced glass transition temperature $T_{rg}=T_g/T_l$ and $\gamma_m = (2T_x - T_g)/T_l$). Positive ΔS_{mix} broadens the composition window for glass formation, and some HEMGs exhibit good GFA with critical sizes ranging from sub-millimeter powders to centimeter-scale bulk samples, varying with chemical composition. Moreover, the GFA of HEMGs is mapped in Fig. 1a using atomic size difference (δ) and mixing enthalpy (ΔH_{mix}), with HEMGs classified into low-, medium-, and high-GFA ones. No definitive conclusion can be drawn that higher δ and more negative ΔH_{mix} tend to enhance the GFA of HEMGs by increasing energy barriers to crystallization[76], even though these two thermodynamic parameters are generally believed to favor amorphous atomic packing by disrupting lattice formation and increasing energy barriers against crystallization. Nevertheless, the plot of the thermodynamic parameter Ω (defined as $T_m\Delta S_{mix}/\Delta H_{mix}$, reflecting the relative contribution of high mixing entropy[78]) versus δ for crystalline HEAs and HEMGs (Fig. 1b) suggests that atomic size mismatch with δ>7.3% is critical for HEMG formation, although HEMGs and HEAs are distinctly divided into two regions in terms of the Ω parameter. In addition, the GFA (D_c) of typical bulk HEMGs (except for Fe-based HEMG ribbons) can be quantitatively correlated with reduced glass

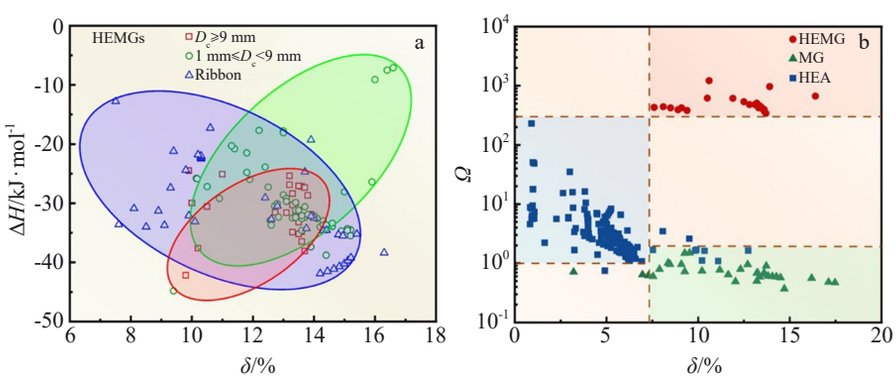

Fig.1 ΔH-δ plot of HEMGs with D_c<1 mm (ribbon), 1 mm⩽D_c<9 mm, and D_c⩾9 mm[76] (a); Ω-δ plot of HEMGs[76], MG, and HEA[78] (b)

transition temperature (T_g/T_l) as well as the calculated parameters such as γ_m (Fig. 2a and 2b). The D_c of typical bulk HEMGs also shows a certain dependence on mixing configuration entropy (Fig. 2c[79]). These findings suggest that, unlike conventional MGs composed of only one or two principal metallic elements, HEMGs, whose composition often deviates from deep-eutectic points, challenge traditional glass-forming rules. Although the GFA of HEMGs basically arises from a synergy of thermodynamic, kinetic, and structural factors (similar to traditional MGs), the sluggish dynamics (slower atomic diffusion) induced by their multi-principal-element nature plays a more significant role in promoting amorphization[46–47,80–81]. Previous studies[20,82–83] suggest that high mixing-configuration entropy is key (but not exclusive) to stabilizing random atomic arrangements in supercooled HEMG-forming melts, thereby increasing their melt viscosity. Combined with the resulting atomic packing frustration, the entropy-driven stabilization hinders ordered crystalline nucleation and thus enhances the GFA of HEMGs[47], essentially raising the crystallization energy barrier and reducing nucleation and growth rates of HEMGs (such as $Ti_{16.7}Zr_{16.7}Hf_{16.7}Cu_{16.7}Ni_{16.7}Be_{16.7}$ alloy)[84]. In addition, high mixing-configuration entropy allows atoms to occupy multiple potential energy wells during quenching, enabling HEMGs to achieve a more relaxed glassy state with dense, disordered structures[85–86].

However, it is worth noting here that high entropy is neither sufficient nor necessary to totally dominate the GFA of some HEMGs, as displayed in Fig. 2. For example, despite its high ΔS_{mix} and thermal stability, the $Fe_{20}Si_{20}B_{20}Al_{20}Ni_{20}$ HEMG-forming supercooled melt exhibits poor GFA, as indicated by its reduced critical casting size D_c[87–88]. This unusual inverse correlation between thermal stability and GFA may be attributed to other crucial factors controlling the crystallization of HEMG-forming liquids, as reviewed in Section 4[26,89–92].

3 Unusual Structural Relaxation Behavior of HEMGs

Owing to the so-called "high-entropy effect", the promoted sluggish diffusion, chemical disorder, and structural/dynamical heterogeneity may profoundly influence glassy dynamics of HEMGs, manifested as α-relaxation (cooperative, viscous flow near T_g) and β-relaxation (faster, more localized motion). In other words, the enhanced thermal stability against crystallization of HEMGs can be correlated with altered relaxation dynamics[93] compared to conventional MGs. Intriguingly, some unique physical phenomena have been reported for HEMGs, such as decoupling of calorimetric and dynamical glass transitions[94–96], glass-to-glass transitions[97–98], and polyamorphic transitions[85,99–101].

3.1 Decoupling of calorimetric and dynamical glass transitions

The glass transition, a fundamental phenomenon observed in amorphous (non-crystalline) materials such as MGs, remains a critical yet unresolved issue in solid-state physics and materials science[102–104]. It refers to the reversible transition of a viscous liquid into a solid or structurally arrested state upon cooling, marked by changes in mechanical and thermal properties at the glass transition temperature (T_g). For conventional MGs, the calorimetric glass transition temperature T_g (measured by differential scanning calorimetry, DSC) and dynamical glass transition temperature T_α (extracted from mechanical spectroscopy, linked to α-relaxation or co-operative diffusion) usually show the same trend[105–106]. Therefore, as suggested in previous work, the calorimetric and dynamic glass transitions may follow the same structural arrest mechanism[107]. However, Jiang et al[94] recently reported the decoupling as an unusual phenomenon in newly developed HEMGs when employing the combination of DSC and dynamic mechanical analysis (DMA) to comparatively study the glass transition of three prototypical systems, including La(Ce) -Ni-Al, Pd(Pt) -Cu-Ni-P, and Ti(Zr) -Cu-Ni-Al. By comparison, the La(Ce) -Ni-Al HEMG shows the highest T_α and maximum α-relaxation activation energy (E_α=267.6 kJ/mol) but a moderate calorimetric T_g, indicating that sluggish dynamics of the HEMG accompanies the decoupling of calorimetric and dynamical glass transition. It is proposed that high configurational entropy delays α-relaxation in the La(Ce)-based HEMGs. Moreover, from the viewpoint of atomic-scale structure, high mixing configurational entropy reduces its dynamical and spatial structural heterogeneity, as indicated by

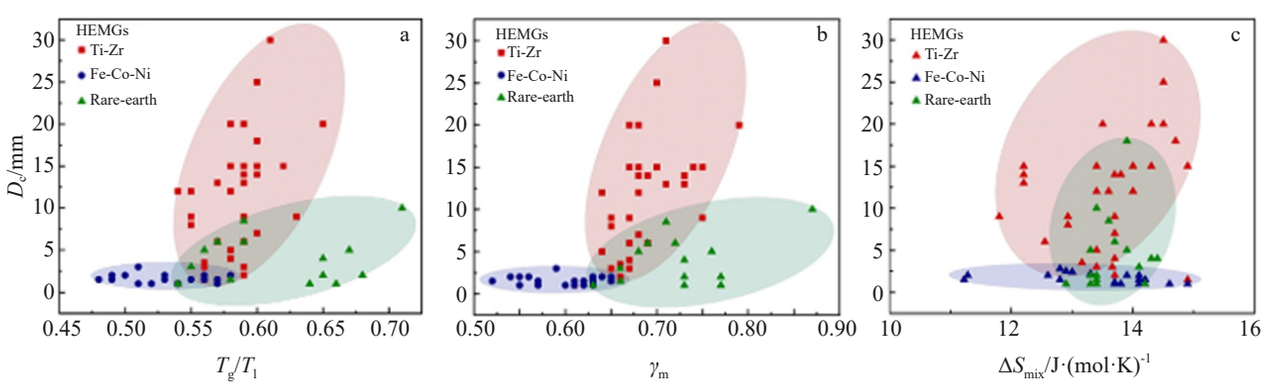

Fig.2 Correlation of critical size D_c for high-entropy glass formation with reduced glass transition temperature T_g/T_l (a), γ_m parameter (b), and mixing configuration entropy ΔS_{mix} (c)[76,79]

smaller, more homogeneous nanoscale domains. Furthermore, Li et al[95] performed molecular dynamics simulations on model HEMGs to elucidate the mechanism underlying the decoupling of calorimetric and dynamical glass transitions as a function of alloy stoichiometry. The results show that atomic-scale mismatch entropy (S_E) plays a critical role in decoupling vitrification kinetics and α-relaxation in HEMGs, in addition to the high configurational entropy (S_C). As shown in Fig.3a, the decoupling phenomenon occurs only when both S_C and S_E are relatively high (e. g., Ti-Zr-Hf-Nb-Ta system), whereas T_g is essentially correlated to T_α for systems with low S_E (e.g., Co-Ni-Cr-Fe-Mn). Microscopically, high S_E related to atomic size differences retards kinetics of α-relaxation associated with long-range sluggish diffusion and reduces dynamic heterogeneity.

More recently, Li et al[96] further examined the effect of pressure, another versatile thermodynamic variable, on anomalous decoupling behavior in several prototypical MGs and HEMGs via molecular dynamics simulations. They found that pressure can significantly depress atomic diffusion and structural α-relaxation, thereby promoting decoupling of the glass transition. For instance, under atmospheric/low-pressure conditions, vitrification kinetics is typically coupled with α-relaxation in Co(Ni)CrFeMn MGs, but it is decoupled at pressures above 10 GPa. Furthermore, a novel phase diagram and a simple criterion, $S=H(S_C-1.36R)\cdot\max(S_E/-0.564, P/10)$, where H is Heaviside step function, R is the gas constant, and S_E and P are regulated by a maximum function, were proposed[96] to describe glass transition coupling/decoupling, framed by configurational entropy, mismatch entropy, and pressure. Apparently, when $S\geqslant 1$, the enhanced sluggish atomic diffusion within MGs will increase the energy barrier for α-relaxation in the potential energy landscape (PEL), causing decoupling of vitrification kinetics and α-relaxation in HEMGs (Fig. 3b). That is, the coupled and decoupled MGs can be separated in terms of the criterion S boundary value of 1.

All in all, the decoupling of the calorimetric and dynamical glass transitions is crucial for understanding the glassy nature and dynamics of HEMGs. Moreover, high configurational entropy, combined with atomic-scale mismatch and high pressure, should play a vital role in tuning the atomic structure, inducing sluggish atomic diffusion, and enhancing the properties of HEMGs[80].

3.2 Glass-to-glass transitions induced by high-entropy effect

Luan et al[97] experimentally investigated an unusual glass-to-glass transition to a low-energy amorphous state in the equiatomic HEMG NbNiZrTiCo during heating, characterized by a prominent exothermic peak even larger than that of subsequent crystallization at higher temperatures (Fig. 4a). According to Ref.[97], this unique physical process is accompanied by a dramatic atomic rearrangement with short- and medium-range ordering without chemical segregation. The authors proposed that the high-entropy effect thermodynamically enables glass-to-glass transitions from high-energy to low-energy glass states during heating[98]. That is, high entropy can trap MGs in high-energy states during rapid cooling, enabling glass-to-glass transitions upon reheating, a distinct phenomenon from minor local adjustments in typical relaxation. More interestingly, HEMG, stabilized in a relatively high-energy state due to the glass-to-glass transition, exhibits enhanced mechanical properties (e. g., modulus and hardness), with effects that are more pronounced than those observed with thermal cycling or mechanical deformation[97]. This sharply contrasts with low-entropy MGs, where such transitions are absent (Fig.4b). These findings suggest that the high-entropy effect creates a new pathway for tailoring glassy states and improving MG properties.

3.3 Continuous polyamorphic transitions (CPTs)

According to prior works[99–100], MGs can undergo CPT, a gradual evolution through multiple polyamorphous states (same composition, varying density/energy) without abrupt phase separation. Recently, the polyamorphic transition in HEMGs has attracted great attention due to its unique continuous and high-order characteristics. Cao et al[101] firstly reported that while polyamorphic transitions (PTs) in conventional MG typically exhibit pronounced first-order characteristics, the CPT in $Ti_{20}Zr_{20}Hf_{20}Cu_{20}Ni_{20}$ HEMG exhibits asymptotic and continuous progression with high-

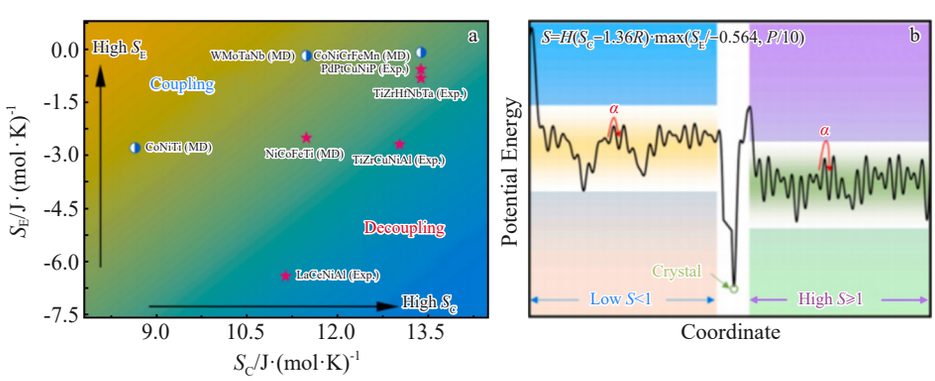

Fig.3 Generic phase diagram of glass transition coupling-decoupling spanned by mixing entropy S_C and mismatch entropy S_E (blue and pink symbols represent MGs with glass transition coupling and glass transition decoupling, respectively)[95] (a); schematic illustration of PEL with criterion S[96] (b)

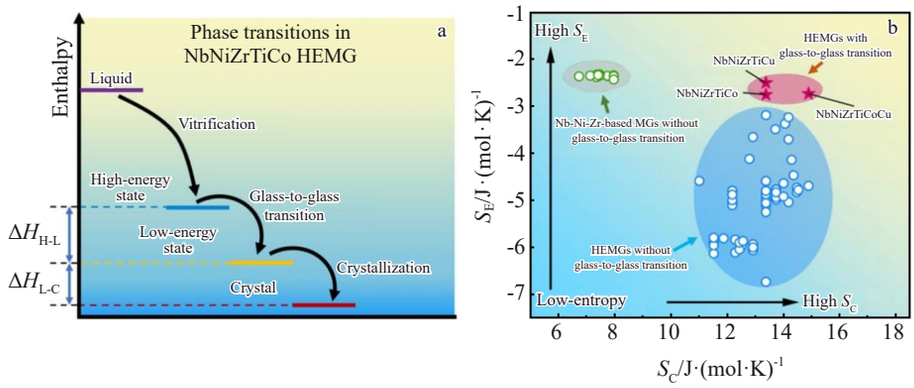

Fig.4 Glass-to-glass transition in HEMGs[97]: (a) transition path of NbNiZrTiCo HEMG and (b) effect of entropy on the glass-to-glass transition

order-like attributes of phase transformation. Using small-angle neutron scattering, extended X-ray absorption fine structure, and reverse Monte Carlo simulations, the authors examined in detail the evolution of atomic structure during CPT. The experimental results show that this CPT is associated with nanoscale chemical heterogeneity and short-range atomic ordering, without a sudden reduction in volume or energy. Unlike discrete polyamorphism in conventional MGs, CPT's continuity in HEMGs stems from high-entropy-driven bond dissociation and chemical gradients. Notably, this high configurational entropy-induced continuous transformation involves a wider spectrum of accessible atomic packing configurations, while the absence of locally favorable structures and chemical heterogeneity enhances the flexibility and adjustability of atomic arrangements and limits the distance and frequency of atomic diffusion. Based on Landau theory, Cao et al[101] further proposed a phenomenological model that correlates CPT with the roughening of the PEL induced by the high-entropy effect (Fig.5a).

To unveil the underlying structural origin in HEMGs, Yang et al[85] systematically studied PT behavior in 62 Zr-Ti-Hf-Co-Ni-Cu-Nb-Al-based HEMGs. The experimental investigations further indicate that the polyamorphic transition is closely correlated with the complexity of the parent crystalline phase. Crystallized HEMGs capable of polyamorphic transitions always possess a multiphase structure (e.g., B2+Laves or bcc phases), while systems without polyamorphic transitions are mostly single-phase (e. g., B2). Furthermore, taking into account entropy-induced structural ordering, namely the formation of medium-range order (MRO), the researchers suggested that polyamorphic transitions within the glassy state are essentially the inheritance and evolution of two competing short-range orders (SROs) from the melt (Fig.5b).

The above compelling experimental findings provide the foundation for establishing the "entropy-structure-property" relationship for HEMGs, which is crucial for understanding their glassy nature and guiding alloy design to optimize glassy properties.

3.4 Mechanical relaxation spectra of HEMGs

According to the previous reports[108], high configurational entropy significantly affects the glassy dynamics of HEMGs. Compared to traditional MGs, HEMGs generally exhibit slower, more heterogeneous dynamics manifested as α-relaxation and β-relaxation in mechanical relaxation spectra[109–111].

In previous works[112–113], two key techniques were employed to probe glassy dynamics in HEMGs: static stress relaxation (time-dependent stress decay under constant strain) and dynamic relaxation spectroscopy (e. g., DMA, which reveals frequency- and temperature-dependent responses via oscillatory stress/strain). These techniques complement each other by accessing the same underlying mechanisms: structural heterogeneity and mobile "liquidlike zones" from both static (time-domain) and dynamic (frequency-domain) perspectives[114]. The process of static stress relaxation in HEMGs is characterized by non-exponential decay, often fitted by the Kohlrausch-Williams-Watts (KWW) function: $\sigma(t)=\sigma_0\exp[-(t/$

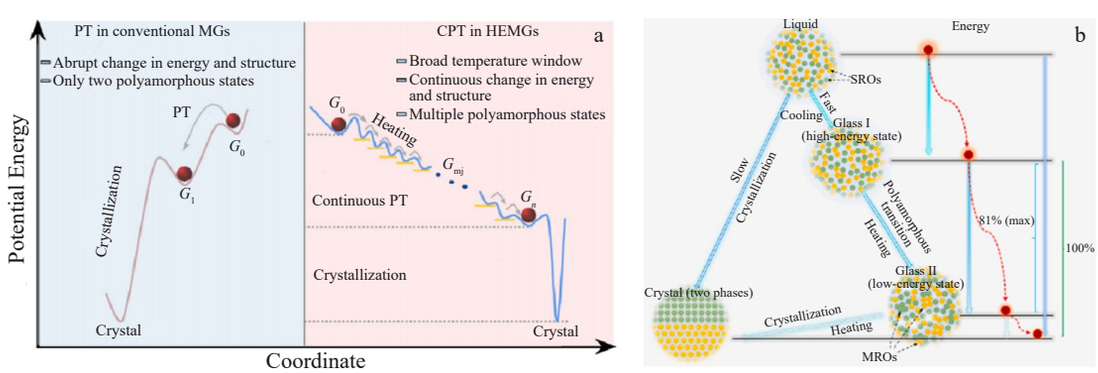

Fig.5 Potential energy topography characteristics of CPT in HEMGs and PT in conventional MGs[101] (a); proposed mechanism[85] (b)

$\tau)^{\wedge}\beta_{KWW}]$, where σ_0 is initial stress, τ is the characteristic relaxation time, and β_{KWW} (<1) quantifies dynamical heterogeneity (lower β indicates broader relaxation time distributions). Moreover, β_{KWW} parameter highlights stress-temperature interplay that accommodates viscoelastic deformation. For instance, according to the recent work by Duan et al[114–115], normalized stress $\sigma(t)/\sigma_0$ in $Pd_{20}Pt_{20}Cu_{20}Ni_{20}P_{20}$ HEMG exhibits a rapid initial drop (25% – 50% within minutes) followed by sluggish decay, approaching residual stress σ_r after extended time. This static probe quantifies the fraction of liquidlike zones (f_{LZ})/mobile regions responsible for 25% – 50% of the initial stress decay, thereby directly linking relaxation to aging and structural evolution. Moreover, they found that this stress relaxation, spanning a wide temperature range (below T_g=572 K), is governed by structural heterogeneity, arising from coexisting rigid (tightly bonded icosahedral clusters) and soft (loosely packed, free-volume-rich) regions. Notably, this relaxation behavior can be amplified by high entropy, which elevates activation barriers (unbiased $\Delta Q\approx$3.65–6.07 eV, (74–123)k_BT_g) and reduces flow unit sizes by retarding diffusion and confining motions to icosahedral networks. Non-exponential statics decays (low β_{KWW}), but mirror broad dynamics peaks, arising from distributed activation energies (200–600 kJ/mol)[105,116]. Furthermore, theoretical models for Pd-based HEMGs decompose relaxation into thermal (static aging) and athermal (stress-driven) contributions, thereby explaining how dynamic heterogeneity predicts static flow resistance[117–118].

Prior DMA investigations reveal that β-relaxation, driven by excess free volume in liquid like zones of HEMG, is typically stronger and broader, with $E_\beta/k_BT_g\approx$30–45, compared with 20 – 30 for conventional MGs. In TiZrHfCu-based HEMGs, β-relaxation shows higher activation energies and smaller stretching exponents (β_{KWW}, 0.4–0.6), indicating greater dynamical heterogeneity and lower defect concentrations (via quasi-point defect models)[82,119]. This indicates that a high mixing-configuration entropy tends to minimize defect proliferation in HEMGs. Duan et al[115] found that the prominence of β-relaxation in La-Ce-Y-Ni-Al-Co HEMGs is closely correlated with the multivalence of constituent elements: greater variety and concentration of multivalent elements (e.g., Ce^{3+}/Ce^{4+}, Y^{2+}/Y^{3+}) correspond to more pronounced β-relaxation. In other words, multivalence-induced variations in atomic spacing lead to the formation of more weakly bonded (soft) regions, which, in turn, promote β-relaxation.

4 Crystallization Behavior of HEMGs

Generally, crystallization is a critical process for glassy materials, as it determines their applicability in structural components, magnetic devices, and other fields that require fully amorphous or partially nanocrystallized structures. Specifically, controlled devitrification of HEMGs can effectively tailor their microstructures to improve their inherent properties[44,120–121]. It is widely accepted that the composition design of HEMGs, typically featuring multiple near-equimolar principal elements, leverages high configurational entropy to stabilize disordered atomic arrangements with complex atomic interactions. High entropy reduces the Gibbs free energy difference between the liquid and crystal states, thereby endowing HEMG-forming alloys with greater thermal stability against crystallization[25,46,122–123]. Therefore, a fundamental understanding of the crystallization in HEMGs and their supercooled melts is scientifically and technologically important.

4.1 Typical crystallization behavior of HEMGs

In previous studies[4,24], the crystallization behavior of HEMGs has been extensively investigated using DSC, X-ray diffraction (XRD), transmission electron microscopy, and other methods. Upon heating, HEMGs typically exhibit distinct exothermic peaks in DSC curves, indicating multiple crystallization stages. For instance, $Zr_{40}Hf_{10}Ti_4Y_1Al_{10}Cu_{25}Ni_7Co_2Fe_1$ HEMG exhibits up to five crystallization stages at low heating rates (⩽20 K/min) [124]. Nevertheless, compared to conventional MGs, crystallization in HEMGs follows similar pathways but is modulated by composition, processing conditions, and high configurational entropy. Unlike conventional MGs, which often follow eutectic or polymorphic routes, HEMGs generally favor primary crystallization with entropy-mediated transitions due to their multi-principal-component nature.

In principle, primary crystallization is diffusion-controlled, involving the formation of a single crystalline phase with a composition different from that of the amorphous matrix. As demonstrated in Ref. [120], this dominant mechanism in typical $(Fe_{0.25}Co_{0.25}Ni_{0.25}Cr_{0.125}Mo_{0.125})_{100-x}B_x$ HEMG systems involves rapid nucleation of nanocrystals (e. g., bcc or fcc phases) from the amorphous matrix. The resulting high nucleation rates yield nanoscale precipitates and dense grain boundaries, which are favorable for enhancing the soft magnetic properties of Fe-based HEMG at high frequencies. In theory, high entropy promotes the growth of pre-existing nuclei in HEMGs. Crystallization kinetics studies of HEMG-forming supercooled liquids based on the Kolmogorov-Johnson-Mehl-Avrami model yield Avrami exponents n>2.5 (indicating three-dimensional growth and increasing nucleation) and $n\approx$ 4 (indicating interface-controlled growth). Moreover, it has been shown that incubation periods exhibit chemical short-range order (CSRO), thereby lowering the energy barriers to nucleation[125–126]. Nevertheless, Ding et al[122] reported an Avrami exponent<1.5 for $Ti_{20}Zr_{20}Cu_{20}Ni_{20}Be_{20}$ HEMG, suggesting diffusion-controlled growth of quenched-in nuclei across all events.

4.2 Unique factors controlling crystallization of HEMGs

As reviewed in the section above, the high-entropy effect may induce unique structural relaxation behavior (glass-to-glass transition, PT, etc). The variation in structural and energetic states associated with these physical processes can significantly affect subsequent crystallization reactions in HEMGs[26,120]. According to previous work[97], the glass-to-glass transition, a unique pre-crystallization phenomenon in HEMGs, typically involves structural relaxation, massive heat release, and atomic reordering (short- to medium-range) with-

out compositional segregation or full devitrification. Luan et al[97] investigated the crystallization of the $Nb_{20}Ni_{20}Zr_{20}Ti_{20}Co_{20}$ HEMG-forming liquid and found that the glass-to-glass transition, which stems from high entropy-induced reconfiguring atomic packing, not only improves modulus and hardness but also acts as a "buffer", delaying subsequent crystallization. Nevertheless, continuous polyamorphic transitions cause the amorphous structure of HEMGs to evolve between low- and high-density states, potentially leading to polyamorphic crystallization in their stabilized supercooled liquids and yielding multiple metastable phases.

Additionally, microalloying effectively modifies the crystallization behavior of HEMGs (similar to that of conventional MGs)[127]. According to the work by Hammid et al[128], adding Al to the $Zr_{20}Cu_{20}Ni_{20}Ti_{20}Hf_{20}$ HEMG diversifies the crystallization stages in the supercooled liquid region, and the structural heterogeneity is somewhat enhanced by the introduction of additional energy-level sites and a more complex evolution. That is, structural heterogeneity, amplified by microalloying, creates varied energy landscapes that promote staged crystallization and influence relaxation (α/β types). In GdYScAlCo and $Ti_{20}Zr_{20}Cu_{20}Ni_{20}Be_{20}$ HEMGs[129–130], this heterogeneity results in "strong" kinetic behavior, favoring crystallization resistance in supercooled liquids with stable activation energies across devitrification events.

5 Unique Mechanical Properties of HEMGs

As is well known, the disordered atomic structure, lacking long-range periodicity, endows conventional MGs with exceptional mechanical properties, such as high strength and elasticity[131–134]. Recent experimental and simulation investigations[42,135–136], however, show that HEMGs, which incorporate multiple (usually five or more) principal elements in near-equiatomic ratios to leverage high configurational entropy, exhibit enhanced stability and tunability compared to conventional MGs (typically based on one or two principal elements with additives). This section reviews the mechanical properties (strength and plasticity) of HEMGs, highlighting differences from conventional MGs.

According to previous work[131–132,137], conventional MGs typically exhibit extremely high strength due to the absence of defects, such as dislocations and grain boundaries, in crystalline alloys. For instance, typical compressive tests show yield strengths of 1500 – 2000 MPa and elastic moduli of 80 – 100 GPa, as seen in Zr-based systems such as $Zr_{41.2}Ti_{13.8}Cu_{12.5}Ni_{10}Be_{22.5}$ (around 1800 MPa), with hardness values of generally 5–8 GPa[138]. However, they are often brittle at room temperature, with limited plasticity (plastic strain <2%) due to localized shear banding, which can lead to catastrophic failure. It is worth noting that structural manipulation via various thermomechanical treatments (e. g., physical aging) yields minor improvements (e. g., hardness increase<10%) without major phase transitions in HEMGs[99–100,139–140].

By comparison, HEMGs benefit from chemical complexity and high entropy, often causing superior mechanical performance. Table S2 provides a comprehensive overview of the yield strength (σ_y), fracture strength (σ_f), and plasticity (ε_p) of various HEMGs at room temperature, highlighting the wide range of achievable mechanical responses. The plastic strain varies remarkably across different HEMGs, ranging from approximately 16.8% for $Zr_{33}Hf_8Ti_6Cu_{32}Ni_{10}Co_5Al_6$ bulk metallic glass (BMG)[141] to near zero for most Fe-containing HEMG ribbons (e. g., $Fe_{20}Co_{20}Ni_{20}Cr_5Mo_{15}P_{10}B_{10}$)[142]. Specifically, the plasticity of Ti-Zr-based HEMG typically rises from approximately 2.3% (equiatomic $Ti_{20}Zr_{20}Hf_{20}Be_{20}Cu_{20}$[16]) to approximately 7.7% ($Ti_{30}Zr_{30}Be_{20}Al_5Cu_{7.5}Ni_{7.5}$[38]), indicating the role of subsequent chemical alloying in boosting plasticity of HEMGs. Moreover, Table S2 shows that this chemical variation simultaneously increases the yield strength from approximately 1.9 GPa to approximately 2.2 GPa. In contrast, Fe-based HEMGs (e. g., $Fe_{25}Co_{25}Ni_{25}(B_{0.7}Si_{0.3})_{25}$[143]) exhibit extremely high strength (as high as approximately 3.7 GPa) but limited plastic strain (1.7%). However, previous work[24,144] also reported that atomic-scale structural rearrangements associated with HEA core effects (sluggish diffusion and/or CSRO) can markedly reduce brittleness in some HEMGs, thereby enabling more distributed shear transformations and larger plastic strains (>5%). For instance, with the assistance of external stimuli, cryogenic cycling increases the plastic strain of $Ti_{20}Zr_{20}Hf_{20}Be_{20}Cu_{20}$ HEMG from 0.62% to 5.38%[135].

The plasticity actually varies significantly across HEMGs, suggesting that other key factors may control their plasticity, with the underlying mechanism differing from that of conventional MGs. Indeed, the parameter of B/G or Poisson's ratio is frequently used previously to evaluate the plasticity of conventional MGs: a lower B/G ratio (indicating a higher Poisson's ratio, ν) generally corresponds to better plasticity. In fact, the plastic behavior of some HEMGs follows this criterion. For example, Zhao[145] and Gao[37] et al reported that both $Sr_{20}Ca_{20}Yb_{20}Mg_{20}Zn_{10}Cu_{10}$ and $Sr_{20}Ca_{20}Yb_{20}Mg_{20}Zn_{20}$ BMGs exhibit extremely limited plasticity, while the values of their Poisson's ratio are determined to be 0.282 and 0.283, respectively (consistent with conventional brittle MGs, ν<0.3).

Nevertheless, according to the works by Sun[146] and Wang[147] et al, a high Poisson's ratio corresponds to pronounced structural heterogeneity, which remarkably influences initial shear stability, thus favoring multiple distributed shear banding (homogeneous-like deformation). In addition, numerous prior works indicate that high configurational entropy tends to decrease structural heterogeneity and promote sluggish diffusion in HEMGs[144], so the superior plasticity in some HEMGs cannot be attributed solely to initial structural heterogeneity. However, previous investigations[41,75,148] indicate that high configurational entropy drives the formation of high-potential-energy inherent structures, thereby endowing HEMGs with both the complexity and flexibility of atomic-scale structures and/or structural heterogeneity. Along these lines, one can envision that the in-situ evolution of structural heterogeneity under stress may be a unique mechanism for achieving superior plasticity in HEMGs. However, much more experimental or theoretical analyses are needed in future work

to check this critical issue of plastic deformation mechanism.

In general, HEMGs outperform conventional MGs in strength, hardness, and thermal-mechanical stability, owing to entropy-driven structural flexibility and evolution (e. g., polyamorphism or glass-to-glass transitions[97,101]) that are absent or minimal in conventional systems. That is, conventional MGs offer reliable baseline properties but lack tunability for extreme performance enhancements.

6 Atomic-Scale Structure and Structural Heterogeneity in HEMGs

As an amorphous subclass of HEAs, HEMGs incorporate multiple principal elements (typically five or more) in near-equiatomic proportions, leveraging high configurational entropy to stabilize high-energy glassy phases[19,73,77,79,149]. Combined with chemical complexity, this imparts HEMGs with unique structural features and enhanced tunability compared to conventional MGs, leading to superior thermal stability and mechanical properties[85,120,150–153]. Structural heterogeneity, intrinsic to MGs and underpinning their inherent properties and phenomena, such as β-relaxation and plastic deformation, can be modulated by the high-entropy effect in ways distinct from those in conventional MGs[154]. This section briefly reviews previous experimental and simulation results on the atomic-scale structure, structural heterogeneity, and their evolution under external stimuli (such as temperature, stress, or pressure).

For conventional MGs, the atomic structure is typically characterized by a dense, random packing of atoms, with SROs as local polyhedral clusters. Zr-based systems (e. g., $Zr_{64.13}Cu_{15.75}Ni_{10.12}Al_{10}$) feature icosahedral clusters dominated by Zr-Zr/Zr-Cu pairs, typically involving coordination numbers of 12–13, as revealed by pair distribution functions (PDF) and structure factors from synchrotron X-ray diffraction[155–156]. Meanwhile, MRO forms networks through interconnected clusters beyond SRO, which contribute to the glass transition and crystallization[157–158]. It is worth noting that conventional MGs generally form stable low-energy atomic-scale structures, showing minimal drastic transitions under external stimuli (pressure or moderate heating). For instance, the atomic-scale evolution can be linked to thermal expansion and contraction of the first coordination shells due to atomic exchange (e.g., outward migration of larger atoms), which can eventually lead to relaxation and nanocrystallization at sufficiently high temperatures[159–161].

By comparison, HEMGs exhibit more complex atomic structures due to their multi-component nature, which, however, introduces high chemical disorder and atomic packing frustration[80,95,162–167]. For instance, in the $Zr_{20}Nb_{20}Cu_{20}Ni_{20}Ti_{20}$ HEMG, the as-quenched state leads to nearly random nearest-neighbor distributions, with high configurational entropy stabilizing a metastable high-energy glass[168]. However, PDF analysis reveals variable CSRO: random neighbors are replaced by energetically favored ones upon heating, leading to bond switching and structural crossovers[169–170]. In the NbNiZrTiCo HEMG, SRO/MRO ordering increases during glass-to-glass transitions, as indicated by synchrotron XRD results showing shifts in PDF peaks and narrowing of structure factor peaks, attributed to significant reordering rather than compositional phase separation[97]. High entropy depresses the glass transition by promoting homogeneous yet flexible structures, with higher configurational entropy enabling greater atomic cooperativity and ordering potential. Notably, these changes in the short/medium-range ordered atomic structures in HEMGs are much stronger than those related to typical structural relaxation[65,133–134,171–174], glass-to-glass, or liquid-to-liquid transitions[99–100,140]. Under sufficiently high pressure, $Ti_{16.7}Zr_{16.7}Hf_{16.7}Cu_{16.7}Ni_{16.7}Be_{16.7}$ HEMG also exhibits enhanced flexibility from chemical complexity, resulting in SRO altering dramatically and thus the occurrence of a local structural crossover at around 20 GPa[84]. Overall, HEMGs exhibit distorted clusters and variable bond lengths, driven by differences in atomic sizes and mixing enthalpies among elements. Thus, the primary distinction in atomic-scale structure between HEMGs and conventional MGs lies in the degree of chemical/structural disorder. Conventional MGs have relatively uniform SRO with preferred atomic pairs and stable low-energy configurations, whereas HEMGs exhibit higher initial disorder than CSRO, enabling tunable transitions (glass-to-glass or pressure-induced crossovers) that are absent in their conventional counterparts[97,175].

Structural heterogeneity refers to spatial variations in atomic density, order, or composition that significantly affect properties such as plasticity and relaxation in MGs[176]. In conventional MGs, heterogeneity is typically modeled via core-shell structures (solid-like elastic matrices encasing liquidlike flow units) [105], as evidenced by nanoindentation mapping of shear modulus and viscosity variations in Zr-based BMGs[32]. It arises from the disordered atomic structure inherited from supercooled liquids, which influences anelastic deformation, shear band formation, and ductility, with icosahedral MRO networks contributing to heterogeneous atomic motions[47,177].

In HEMGs, the high-entropy effect introduces competition among entropy, enthalpy, and atomic stress, leading to more pronounced heterogeneity in local environments than conventional MGs, where heterogeneity is more static and less tunable. For instance, structural heterogeneity in NbNiZrTiCo HEMG can be amplified by chemical complexity, manifesting as variable CSRO and dynamic structural crossovers without compositional inhomogeneity, as evidenced by atom-probe tomography experiments that show uniform elemental distribution[97]. Gu et al[178] reported dynamical structural heterogeneity in $Ti_{20}Zr_{20}Hf_{20}Be_{20}Cu_{7.5}Ni_{12.5}$ HEMG using high-speed nanoindentation experiments, revealing a pronounced anelastic deformation associated with non-affine deformation in loose-packing regions. It is revealed that the as-cast high-entropy BMG exhibits the lowest fraction of loose-packing regions among conventional Ti-based BMGs with similar elements, indicating lower structural heterogeneity[34,73,179]. Moreover, through systematic studies on the calorimetric and

dynamical glass transitions in three typical HEMGs ($La_{27.5}Ce_{27.5}Ni_{20}Al_{25}$, $Pd_{20}Pt_{20}Cu_{20}Ni_{20}P_{20}$, and $Ti_{25}Zr_{25}Cu_{20}Ni_{20}Al_{10}$), Jiang et al[94] reported that high mixing configurational entropy decreases dynamic and spatial heterogeneities and sluggish diffusion, i. e., one of HEA "core effects", which causes a depressed dynamical glass transition phenomenon; as a result, the so-called decoupling between calorimetric and dynamical glass transitions is revealed for the studied HEMGs with moderate calorimetric T_g. This is important for understanding the effect of entropy on the structure and properties of MGs and for designing new materials with robust physical and mechanical properties. According to the prior work by Duan et al[115], who carried out DMA and stress relaxation experiments on a series of HEMGs, an intrinsic relationship between the fraction of liquidlike zones and the spectrum of relaxation modes strongly supports that a spatial distribution of relaxation-time zones allows HEMGs to be more or less liquidlike in nature (similar to MGs). More interestingly, their experimental results indicate that high mixing entropy leads to sluggish diffusion in liquid dynamics, as suggested in other works[94,180]. Theoretically, the molecular dynamics simulation with machine learning proposed by Liu et al[157] further revealed the stress-driven evolution of dynamic structural heterogeneity in $Cu_{20}Zr_{20}Ni_{20}Ti_{20}Pd_{20}$ HEMG, identifying liquidlike regions associated with low five-fold symmetry, low coordination packing, and pronounced CSRO. Compared with conventional MGs, this HEMG exhibits a smaller creep activation volume, fewer active atoms, and slower dynamics.

Overall, the unique atomic-scale features of HEMGs (including variable CSRO and enhanced heterogeneity) offer greater structural flexibility, enabling tailored responses to external stimuli and improved properties (hardness, elastic modulus, and crystallization resistance). In contrast, conventional MGs provide only a baseline of stability and lower adaptability. These differences highlight configurational entropy as a key design parameter for advanced amorphous materials, with potential applications in high-performance alloys for extreme environments. Ongoing research continues to refine atomic-scale models to bridge structure-property gaps in both material classes.

7 Summary and Outlook

HEMGs represent a novel material class that merges the compositional complexity of HEAs (typically featuring five or more principal elements in near-equiatomic ratios) with the amorphous structure of conventional MGs. This combination yields materials with high configurational entropy and no long-range atomic order, exhibiting unique properties superior to those of traditional MGs or HEAs in certain respects.

Developed from HEAs (pioneered around 2004) and MGs (1960s), HEMG research has accelerated rapidly since the first report in 2011. To date, over 100 HEMGs have been developed, often based on common elemental systems such as Ti-Zr-Hf-Cu-Ni-Be, Fe-Co-Ni-based, Pt-Pd-based, and rare-earth-based alloys. While the GFA of HEMGs is influenced by factors such as atomic size mismatch (δ), mixing enthalpy (ΔH), and configurational entropy (ΔS). Empirical rules suggest that HEMGs with moderate negative ΔH and appropriate δ exhibit higher GFA, enabling the formation of bulk samples via methods such as copper mold casting.

Moreover, arising from their unique multi-principal-element alloy design, the resultant "high-entropy effect" stabilizes amorphous structures, suppresses crystallization, prolongs stress relaxation, and slows relaxation dynamics by promoting sluggish diffusion and chemical disorder, as well as the heterogeneity-driven evolution of a hierarchical dynamic microstructure. More interestingly, despite lacking long-range atomic order (similar to conventional MGs), HEMGs exhibit additional structural evolution complexity: decoupled glass transition, potential glass-to-glass (polyamorphic) transitions, and CPT during reheating, enabling tunable atomic rearrangement, interaction, and structural (chemical and/or topological) heterogeneity.

Previous work has underscored that high entropy alters glass dynamics and structural heterogeneity, thereby promoting the thermal/mechanical stability and GFA of HEMGs and enabling tunable relaxation for advanced applications such as structural materials. However, several critical issues remain to be resolved: refine atomic-scale models to bridge the structure-property gaps in high-entropy tailored MGs; optimize alloy design via microalloying to balance GFA, nanocrystallization, and the structural/functional properties of HEMGs; fundamentally understand the impact of entropy on atomic-scale chemical/topological ordering, sluggish diffusion, hierarchical glassy dynamics, phase selection, and the formation of glass or nanocrystal-reinforced glass matrix composites in HEMG-supercooled liquids; clarify how multivalent elements affect the coupling between large-scale atomic/cluster cooperative rearrangements and local relaxation mode evolution in HEMGs.

Supplement

Table S1 Composition, critical casting thickness (D_c), glass transition temperature (T_g), crystallization temperature (T_x), melting temperature (T_m), liquidus temperature(T_l), mixing enthalpy (ΔH_{mix}), mixing entropy (ΔS_{mix}), atomic size difference (δ), reduced glass transition temperature (T_{rg}), and γ_m parameter of discovered HEMGs

Composition	D_c/ mm	T_g/ K	T_x/ K	T_m/ K	T_l/ K	ΔH_{mix}/ J·mol^{-1}	ΔS_{mix}/ J·(mol·K)$^{-1}$	δ/%	T_{rg}	γ_m	Ref.
$Ti_{20}Zr_{20}Hf_{20}Be_{20}Cu_{7.5}Ni_{12.5}$	30	632	684	951	1040	−33.2	14.5	13.5	0.61	0.71	[38]
$Ti_{20}Zr_{20}Hf_{20}Be_{20}Cu_{10}Ni_{10}$	25	643	695	948	1066	−31.6	14.5	13.4	0.60	0.70	[38]

Continued table

Composition	D_c/ mm	T_g/ K	T_x/ K	T_m/ K	T_l/ K	ΔH_{mix}/ J·mol^{-1}	ΔS_{mix}/ J·(mol·K)$^{-1}$	δ/%	T_{rg}	γ_m	Ref.
$Ti_{20}Zr_{20}Hf_{20}Be_{20}Cu_5Ni_{15}$	20	644	696	962	1109	−34.8	14.3	13.6	0.58	0.67	[38]
$Ti_{20}Zr_{20}Hf_{20}Be_{20}Cu_{12.5}Ni_{7.5}$	20	644	692	925	1090	−30.0	14.5	13.4	0.59	0.68	[38]
$Zr_{35}Hf_{13}Al_{11}Ag_8Ni_8Cu_{25}$	20	723	802	-	1112	−30.0	13.5	10.0	0.65	0.79	[39]
$Y_{36}Sc_{20}Co_{20}Al_{24}$	20	660	744	-	-	-	-	-	-	-	[80]
$Zr_{35}Hf_{17.5}Ti_{5.5}Al_{12.5}Co_{7.5}Ni_{12}Cu_{10}$	18	725	-	-	1206	−37.6	14.7	10.2	0.60	-	[181]
$Hf_{30}Be_{18}Ti_{16}Zr_{16}Cu_{3.5}Ni_{16.5}$	18	663.66	724.81	1033.28	-	−35.2	13.9	13.5	-	-	[182]
$Ti_{16.7}Zr_{16.7}Hf_{16.7}Cu_{16.7}Ni_{16.7}Be_{16.7}$	15	681	751	1019	1100	−31.6	14.9	13.1	0.62	0.75	[84]
$Ti_{20}Zr_{20}Hf_{20}Be_{20}Ni_{20}$	15	646	701	969	1108	−38.1	13.4	13.7	0.58	0.68	[38]
$Ti_{20}Zr_{20}Hf_{20}Be_{20}Cu_{2.5}Ni_{17.5}$	15	641	692	972	1114	−36.5	14.0	13.6	0.58	0.67	[38]
$Ti_{20}Zr_{20}Hf_{20}Be_{20}Cu_{15}Ni_5$	15	638	694	926	1102	−28.4	14.3	13.3	0.58	0.68	[38]
$Zr_{31}Ti_{27}Be_{26}Cu_{10}Ni_6$	15	610	682	-	1023	−31.9	12.2	13.9	0.60	0.74	[26]
$Zr_{31}Ti_{27}Be_{26}Cu_{10}V_6$	15	610	666	-	1027	−27.2	12.2	13.6	0.59	0.70	[26]
$Zr_{40}Hf_{10}Ti_4Y_1Al_{10}Cu_{25}Ni_7Co_2Fe_1$	14	679	748	-	-	−30.6	13.8	10.5	-	-	[183]
$Zr_{31}Ti_{27}Be_{26}Cu_{10}Ag_6$	14	620	675	-	1057	−27.1	12.2	13.5	0.59	0.69	[26]
$Zr_{31}Ti_{27}Be_{26}Cu_{10}Cr_6$	14	611	678	-	1018	−27.4	12.2	13.7	0.60	0.73	[26]
$Zr_{28}Ti_{24}Be_{23}Cu_9Ni_{10}Ag_6$	14	633	682	-	1074	−30.3	13.7	13.3	0.59	0.68	[26]
$Zr_{31}Ti_{27}Be_{26}Cu_{10}Fe_6$	13	617	685	-	1037	−28.7	12.2	13.8	0.59	0.73	[26]
$Zr_{31}Ti_{27}Be_{26}Cu_{10}Al_6$	13	607	678	-	1060	−31.2	12.2	13.5	0.57	0.71	[26]
$Ti_{20}Zr_{20}Hf_{20}Be_{20}Cu_{20}$	12	630	708	935	1164	−25.4	13.4	13.2	0.54	0.68	[16]
$Zr_{30}Hf_{25}Al_{20}Co_{10}Ni_{10}Cu_5$	12	775	-	-	1337	−42.2	13.6	9.8	0.58	-	[181]
$Ti_{20}Zr_{20}Hf_{20}Be_{20}Cu_{17.5}Ni_{2.5}$	12	641	693	973	1156	−26.9	14.0	13.2	0.55	0.64	[38]
$Pd_{20}Pt_{20}Cu_{20}Ni_{20}P_{20}$	10	580	645	-	820	−25.1	13.4	11.0	0.71	0.87	[15]
$Zr_{28}Ti_{24}Be_{23}Cu_9Ni_{10}Al_6$	9	642	685	-	1087	−34.9	13.7	13.3	0.59	0.67	[26]
$Zr_{31.6}Hf_{13.4}Al_{8.7}Ag_{8.4}Cu_{37.8}$	9	723	789	-	1144	−24.5	11.8	9.9	0.63	0.75	[141]
$(Ti_{37.31}Zr_{22.75}Be_{26.39}Al_{4.55}Cu_9)_{94}Ni_6$	9	632	688	-	1144	−31.6	12.9	12.7	0.55	0.65	[40]
$(Gd_{0.2}Dy_{0.2}Er_{0.2}Co_{0.2}Al_{0.2})_{99.5}Si_{0.5}$	8.5	618	682	-	1049	−32.6	13.6	14.1	0.59	0.71	[47]
$(Ti_{37.31}Zr_{22.75}Be_{26.39}Al_{4.55}Cu_9)_{94}Co_6$	8	633	691	-	1148	−30.5	12.9	12.7	0.55	0.65	[40]
$Zr_{28}Ti_{24}Be_{23}Cu_9Ni_{10}V_6$	7	635	677	-	1064	−31.2	13.7	13.4	0.60	0.68	[26]
$Zr_{28}Ti_{24}Be_{23}Cu_9Ni_{10}Cr_6$	6	637	686	-	1071	−31.2	13.7	13.5	0.59	0.69	[26]
$(Gd_{0.2}Dy_{0.2}Er_{0.2}Co_{0.2}Al_{0.2})_{99}Si_1$	6	624	694	-	1061	−33.0	13.7	14.3	0.59	0.72	[47]
$(Gd_{1/3}Tb_{1/3}Dy_{1/3})_{55}Co_{17.5}Al_{27.5}$	6	617.4	685.9	974.3	1090.6	−35.8	-	-	0.57	0.69	[83]
$(Ti_{41}Zr_{25}Be_{29}Al_5)_{89}Cu_{5.5}Ni_{5.5}$	6	629	683	-	1100	−32.3	12.6	12.8	0.57	0.67	[40]
$Sr_{20}Ca_{20}Yb_{20}Mg_{20}Zn_{10}Cu_{10}$	≥5	351	391	-	642	−7.1	14.5	16.6	0.55	0.67	[37]
$Ti_{20}Zr_{20}Hf_{20}Co_{20}Be_{20}$	5	683	722	-	1187	−34.6	13.4	13.6	0.58	0.64	[184]
$Er_{18}Gd_{18}Y_{20}Al_{24}Co_{20}$	5	635	680	-	953	−34.0	13.3	14.2	0.67	0.76	[46]
$(Gd_{0.2}Dy_{0.2}Er_{0.2}Co_{0.2}Al_{0.2})_{98}Si_2$	5	629	697	-	1133	−33.9	13.9	14.6	0.56	0.68	[47]

Continued table

Composition	D_c/ mm	T_g/ K	T_x/ K	T_m/ K	T_l/ K	ΔH_{mix}/ J·mol^{-1}	ΔS_{mix}/ J·(mol·K)$^{-1}$	δ/%	T_{rg}	γ_m	Ref.
$Zr_{28}Ti_{24}Be_{23}Cu_9Ni_{10}Fe_6$	4	643	694	-	1107	−32.2	13.7	13.6	0.58	0.67	[26]
$Hf_{28}Be_{18}Ti_{17}Zr_{17}Cu_{7.5}Ni_{12.5}$	4	647	688	964	999	−32.5	14.3	13.3	0.65	0.73	[185]
$Hf_{26}Be_{18}Ti_{18}Zr_{18}Cu_{7.5}Ni_{12.5}$	4	649.56	696.15	-	-	−32.5	14.4	13.3	-	-	[186]
$Fe_{76.1}Co_{3.7}Cu_{0.2}B_{3.6}P_{9.4}C_7$	4	-	-	-	-	-	-	-	-	-	[187]
$Hf_{28}Be_{18}Ti_{17}Zr_{17}Cu_{7.5}Ni_{12.5}$	4	641	690	-	-	-	-	-	-	-	[27]
$Ti_{30}Zr_{30}Be_{20}Al_5Cu_{7.5}Ni_{7.5}$	3.5	608	661	-	1085	−32.9	13.2	12.6	0.56	0.66	[40]
$Ti_{48}Zr_{20}Nb_{12}Cu_5Be_{15}$	≥3	-	720	-	-	-	-	-	-	-	[41]
$Ti_{40}Zr_{10}Hf_{10}Ta_{10}Nb_{10}Cu_5Be_{15}$	≥3	-	740	-	-	-	-	-	-	-	[41]
$Ti_{20}Zr_{20}Cu_{20}Ni_{20}Be_{20}$	3	683	729	1076	1161	−30.1	13.4	12.8	0.59	0.67	[122]
$(Gd_{0.2}Dy_{0.2}Er_{0.2}Co_{0.2}Al_{0.2})_{97}Si_3$	3	636	694	-	1147	−34.7	14.1	14.9	0.55	0.66	[47]
$Fe_{0.27}Co_{0.2}Ni_{0.2}Cr_{0.08}Mo_{0.05}P_{0.1}C_{0.04}B_{0.06}$	3	682	733	1184	1333	−25.8	-	-	0.51	0.59	[188]
$Ti_{30}Zr_{30}Be_{20}Al_5Cu_5Ni_5Co_5$	3	598	645	-	1071	−33.7	13.7	12.6	0.56	0.65	[40]
$Fe_{0.25}Co_{0.25}Ni_{0.25}(Si_{0.3}B_{0.7})_{0.25}$	2.8	788	813	-	-	−18.1	12.8	13.0	-	-	[42]
$[Fe_{0.25}Co_{0.25}Ni_{0.25}(Si_{0.3}B_{0.7})_{0.25}]_{99.7}Cu_{0.3}$	2.5	786	805	-	-	−17.9	12.9	13.0	-	-	[42]
$[Fe_{0.25}Co_{0.25}Ni_{0.25}(Si_{0.3}B_{0.7})_{0.25}]_{99.4}Cu_{0.6}$	2.4	784	803	-	-	−17.8	13.0	13.0	-	-	[42]
$(Fe_{1/3}Co_{1/3}Ni_{1/3})_{77.5}Cr_{2.5}(P_{1/2}B_{1/2})_{20}$	2.2	692	721	-	-	−20.8	13.3	11.4	-	-	[84]
$Sr_{20}Ca_{20}Yb_{20}Mg_{20}Zn_{20}$	≥2	353	389	-	630	−9.1	13.4	16.0	0.56	0.67	[37]
$Sr_{20}Ca_{20}Yb_{20}(Li_{0.55}Mg_{0.45})_{20}Zn_{20}$	≥2	-	319	344	559	−7.5	14.5	16.4	0.00	-	[37]
$Ca_{20}Mg_{20}Zn_{20}Sr_{20}Yb_{20}$	≥2	357	390	-	-	−9.1	13.4	16.0	-	-	[189]
$Ti_{20}Hf_{20}Cu_{20}Ni_{20}Be_{20}$	2	717	760	1095	1220	−27.3	13.4	12.5	0.59	0.66	[190]
$Fe_{35}Ni_{20}Cr_{20}Mo_5(P_{0.6}C_{0.2}B_{0.2})_{20}$	2	722	784	-	1350	−28.6	13.9	13.0	0.53	0.63	[21]
$(Fe_{1/3}Co_{1/3}Ni_{1/3})_{80}(P_{1/2}B_{1/2})_{20}$	2	686	712	-	-	−20.3	12.6	11.3	-	-	[191]
$Fe_{25}Co_{25}Ni_{25}(P_{0.5}C_{0.1}B_{0.2}Si_{0.2})_{25}$	2	707	746	-	1227	−24.8	14.1	11.8	0.58	0.64	[43]
$Er_{20}Tb_{20}Dy_{20}Ni_{20}Al_{20}$	2	-	-	-	-	−37.4	13.4	13.9	-	-	[73]
$Er_{18}Gd_{18}Y_{20}Al_{24}Ni_{20}$	2	633	656	-	931	−38.8	13.3	14.4	0.68	0.73	[46]
$Er_{18}Nd_{18}Y_{20}Al_{24}Co_{20}$	2	613	671	-	944	−33.7	13.3	14.3	0.65	0.77	[46]
$Zr_{33}Hf_8Ti_6Cu_{32}Ni_{10}Co_5Al_6$	2	694	773	-	-	−29.2	13.7	10.9	-	-	[38]
$(Fe_{0.27}Co_{0.2}Ni_{0.2}Cr_{0.08}Mo_{0.05}P_{0.1}C_{0.04}B_{0.06})_{99.8}Cu_{0.2}$	2	670	704	1182	1327	−25.6	-	-	0.50	0.56	[188]
$(Fe_{0.27}Co_{0.2}Ni_{0.2}Cr_{0.08}Mo_{0.05}P_{0.1}C_{0.04}B_{0.06})_{99.6}Cu_{0.4}$	2	665	699	1183	1332	−25.5	-	-	0.50	0.55	[188]
$(Fe_{0.27}Co_{0.2}Ni_{0.2}Cr_{0.08}Mo_{0.05}P_{0.1}C_{0.04}B_{0.06})_{99.4}Cu_{0.6}$	2	658	691	1178	1334	−25.4	-	-	0.49	0.54	[188]
$Co_{35}Fe_{35}Nb_5B_{20}P_5$	2	812	878	-	1449	−25.9	11.3	10.2	0.56	0.65	[192]
$Fe_{20}Co_{20}Ni_{20}Cr_{10}Mo_{10}P_{10}B_{10}$	2	705	730	1256	1341	−23.6	-	-	0.53	0.56	[142]
$Ti_{20}Zr_{20}Hf_{20}Cu_{20}Ni_{20}$	1.5	658	711	1247	-	−27.2	13.4	10.5	-	-	[72]
$Ti_{16.7}Zr_{16.7}Nb_{16.7}Cu_{16.7}Ni_{16.7}Be_{16.7}$	1.5	684	739	1066	1218	−26.0	14.9	11.9	0.56	0.65	[190]
$Fe_{30}Ni_{20}Cr_{25}Mo_5(P_{0.6}C_{0.2}B_{0.2})_{20}$	1.5	734	803	-	1396	−29.2	14.1	13.1	0.53	0.62	[21]
$Fe_{25}Co_{25}Ni_{25}(B_{0.7}Si_{0.3})_{25}$	1.5	767	807	-	1391	−18.1	12.8	13.0	0.55	0.61	[143]

Continued table

Composition	D_c/ mm	T_g/ K	T_x/ K	T_m/ K	T_l/ K	ΔH_{mix}/ J·mol^{-1}	ΔS_{mix}/ J·(mol·K)$^{-1}$	δ/%	T_{rg}	γ_m	Ref.
$Fe_{25}Co_{25}Ni_{25}(P_{0.4}C_{0.1}B_{0.3}Si_{0.2})_{25}$	1.5	720	759	-	1263	−23.9	14.2	12.4	0.57	0.63	[43]
$Er_{20}Dy_{20}Co_{20}Al_{20}Gd_{20}$	1.5	610	659	-	-	−32.1	13.4	14.0	-	-	[48]
$Er_{20}Dy_{20}Co_{20}Al_{20}Tb_{20}$	1.5	623	663	-	-	−32.4	13.4	13.7	-	-	[48]
$Gd_{0.2}Dy_{0.2}Er_{0.2}Co_{0.2}Al_{0.2}$	1.5	610	652	-	1053	−32.1	13.4	14.0	0.58	0.66	[47]
$(Fe_{0.27}Co_{0.2}Ni_{0.2}Cr_{0.08}Mo_{0.05}P_{0.1}C_{0.04}B_{0.06})_{99.2}Cu_{0.8}$	1.5	655	679	1194	1343	−25.2	-	-	0.49	0.52	[188]
$(Fe_{0.27}Co_{0.2}Ni_{0.2}Cr_{0.08}Mo_{0.05}P_{0.1}C_{0.04}B_{0.06})_{99}Cu_1$	1.5	654	680	1198	1351	−25.1	-	-	0.48	0.52	[188]
$Co_{40}Fe_{30}Nb_5B_{20}P_5$	1.5	810	872	-	1435	−25.8	11.2	10.2	0.56	0.65	[192]
$Co_{30}Fe_{40}Nb_5B_{20}P_5$	1.5	814	883	-	1469	−25.9	11.2	10.2	0.55	0.65	[192]
$Fe_{20}Co_{20}Ni_{20}Cr_{15}Mo_5P_{10}B_{10}$	1.5	699	723	1215	1316	−23.2	-	-	0.53	0.57	[142]
$Fe_{25}Co_{25}Ni_{25}Mo_5P_{10}B_{10}$	1.2	-	-	-	-	−21.5	13.7	11.8	-	-	[193]
$Fe_{20}Co_{20}Ni_{20}Cr_5Mo_{15}P_{10}B_{10}$	1	708	731	1247	1360	−24.0	-	-	0.52	0.55	[142]
$Ti_{20}Zr_{20}Cu_{20}Ni_{20}Pd_{20}$	1	755	806	1276	1404	−44.8	13.4	9.4	0.54	0.61	[194]
$Fe_{20}Ni_{20}Cr_{25}Mo_{15}(P_{0.6}C_{0.2}B_{0.2})_{20}$	1	800	852	-	1489	−30.6	14.9	13.7	0.54	0.61	[21]
$Fe_{25}Ni_{20}Cr_{25}Mo_{10}(P_{0.6}C_{0.2}B_{0.2})_{20}$	1	752	807	-	1446	−29.9	14.6	13.4	0.52	0.60	[21]
$Fe_{25}Ni_{20}Cr_{30}Mo_5(P_{0.6}C_{0.2}B_{0.2})_{20}$	1	746	797	-	1475	−29.7	14.1	13.1	0.51	0.57	[21]
$Fe_{25}Co_{25}Ni_{25}(B_{0.6}Si_{0.4})_{25}$	1	771	808	-	1358	−17.7	12.9	12.2	0.57	0.62	[143]
$Fe_{25}Co_{25}Ni_{25}(P_{0.5}C_{0.3}B_{0.2})_{25}$	1	674	730	-	1239	−28.1	13.7	15.0	0.54	0.63	[195]
$Fe_{25}Co_{25}Ni_{25}(P_{0.3}C_{0.3}B_{0.4})_{25}$	1	702	749	-	1293	−26.4	13.8	15.9	0.54	0.62	[195]
$Gd_{18}Nd_{18}Y_{20}Al_{24}Co_{20}$	1	588	651	-	923	−33.4	13.3	14.6	0.64	0.77	[46]
$Er_{18}Nd_{18}Gd_{20}Al_{24}Co_{20}$	1	595	624	-	896	−33.7	13.3	14.4	0.66	0.73	[46]
$Er_{20}Dy_{20}Co_{20}Al_{20}Tm_{20}$	1	645	690	-	-	−32.6	13.4	13.6	-	-	[48]
$Ho_{20}Er_{20}Co_{20}Al_{20}Gd_{20}$	1	612	652	-	-	−31.9	13.4	13.8	-	-	[196]
$Ho_{20}Er_{20}Co_{20}Al_{20}Dy_{20}$	1	632	668	-	-	−32.1	13.4	13.6	-	-	[196]
$Ho_{20}Er_{20}Co_{20}Al_{20}Tm_{20}$	1	648	680	-	-	−32.4	13.4	13.4	-	-	[196]
$Gd_{25}Co_{25}Al_{25}Y_{15}Dy_{10}$	1	628	662	-	-	−34.5	12.9	15.2	-	-	[49]
$Gd_{25}Co_{25}Al_{25}Y_{15}Ho_{10}$	1	626	666	-	-	−34.3	12.9	15.1	-	-	[49]
$Gd_{25}Co_{25}Al_{25}Y_{15}Er_{10}$	1	628	665	-	-	−34.6	12.9	15.1	-	-	[49]
$(Gd_{0.2}Dy_{0.2}Er_{0.2}Co_{0.2}Al_{0.2})_{96}Si_4$	1	640	695	-	1186	−35.5	14.2	15.2	0.54	0.63	[47]
$(Ti_{33}Zr_{33}Hf_{33})_{60}(Ni_{50}Cu_{50})_{20}Al_{20}$	Rib.	389	-	987	-	−34.0	14.5	8.5	-	-	[197]
$(Ti_{33}Zr_{33}Hf_{33})_{63.4}(Ni_{50}Cu_{50})_{13.3}Al_{23.3}$	Rib.	377	-	1032	-	−33.6	14.0	7.6	-	-	[197]
$(Ti_{33}Zr_{33}Hf_{33})_{58.8}(Ni_{50}Cu_{50})_{26.6}Al_{16.6}$	Rib.	382	-	959	-	−33.7	14.8	9.1	-	-	[197]
$(Ti_{33}Zr_{33}Hf_{33})_{66.8}(Ni_{50}Cu_{50})_{16.6}Al_{16.6}$	Rib.	364	-	955	-	−30.9	14.3	8.1	-	-	[197]
$(Ti_{33}Zr_{33}Hf_{33})_{63.4}(Ni_{50}Cu_{50})_{23.3}Al_{13.3}$	Rib.	364	-	842	-	−31.3	14.6	8.9	-	-	[197]
$Ti_{30}Zr_{25}Nb_{25}Si_{15}Ga_3B_2$	Rib.	-	-	-	-	−29.1	12.7	12.4	-	-	[198]
$Ti_{20}Zr_{20}Nb_{20}Hf_{20}Si_{15}Ga_3B_2$	Rib.	-	-	-	-	−30.5	14.6	12.8	-	-	[16]
$(FeCoCrNi)_{80}B_{20}$	Rib.	744	788	1395	-	−19.3	13.4	13.9	-	-	[44]

Continued table

Composition	D_c/ mm	T_g/ K	T_x/ K	T_m/ K	T_l/ K	ΔH_{mix}/ J·mol^{-1}	ΔS_{mix}/ J·(mol·K)$^{-1}$	δ/%	T_{rg}	γ_m	Ref.
$(FeCoCrNi)_{80}B_{10}Si_{10}$	Rib.	753	810	1449	-	−17.3	14.5	10.6	-	-	[44]
$Fe_{40}Ni_{40}P_{14}B_6$	Rib.	-	-	-	-	−22.4	9.8	10.3	-	-	[45]
$Fe_{43}Co_{18.5}Ni_{18.5}P_{14}B_6$	Rib.	-	-	-	-	−22.5	11.9	10.3	-	-	[45]
$Fe_{40}Co_{20}Ni_{20}P_{14}B_6$	Rib.	-	-	-	-	−22.4	12.1	10.3	-	-	[45]
$Fe_{35}Co_{22.5}Ni_{22.5}P_{14}B_6$	Rib.	-	-	-	-	−22.2	12.3	10.3	-	-	[45]
$Fe_{30}Co_{25}Ni_{25}P_{14}B_6$	Rib.	-	-	-	-	−22.0	12.5	10.3	-	-	[45]
$Fe_{25}Co_{27.5}Ni_{27.5}P_{14}B_6$	Rib.	-	-	-	-	−21.8	12.5	10.2	-	-	[45]
$Fe_{30}Co_{30}Ni_{30}P_7B_3$	Rib.	-	-	-	-	−12.8	11.4	7.5	-	-	[45]
$Al_{20}Ce_{20}La_{20}Ni_{20}Y_{20}$	Rib.	-	-	-	-	−35.2	13.4	15.4	-	-	[199]
$Gd_{19}Tb_{19}Er_{18}Fe_{19}Al_{25}$	Rib.	590	-	-	-	−24.7	13.3	13.7	-	-	[200]
$Ti_{20}Zr_{20}Nb_{20}Hf_{20}Si_{20}$	Rib.	-	-	-	-	−32.7	13.4	12.6	-	-	[141]
$Nb_{20}Ni_{20}Zr_{20}Ti_{20}Co_{20}$	Rib.	-	-	-	-	−32.1	13.4	9.9	-	-	[97]
$Nb_{20}Ni_{20}Zr_{20}Ti_{20}Cu_{20}$	Rib.	633	-	-	-	−21.2	13.4	9.4	-	-	[97]
$Nb_{16.7}Ni_{16.7}Zr_{16.7}Ti_{16.7}Co_{16.7}Cu_{16.7}$	Rib.	-	-	-	-	−24.4	14.9	9.8	-	-	[97]
$Er_{20}Ho_{20}Dy_{20}Cu_{20}Ni_{20}$	Rib.	397	513	-	-	-	-	-	-	-	[201]
$Zr_{22.5}Ti_{22.5}Hf_{22.5}Ni_{22.5}Ta_{10}$	Rib.	745	812	-	-	−27.4	13.1	9.3	-	-	[22]
$Al_{29}Ni_{29}Y_{29}Co_{10}Si_3$	Rib.	-	-	-	-	−38.4	11.7	16.3	-	-	[23]
$Fe_{20}Co_{20}Ni_{20}Cr_{20}(P_{0.45}B_{0.2}C_{0.35})_{20}$	Rib.	669–693	727–749	-	-	-	-	-	-	-	[80]
$(FeCoNiB_{0.75})_{97}Pt_3$	Rib.	-	-	-	-	-	-	-	-	-	[202]
$Ti_{20}Zr_{20}Hf_{20}Cu_{20}Ni_{20}$	Rib.	694	-	-	-	-	-	-	-	-	[101]
$(FeCoNiMn_{0.25}Al_{0.25})_{75}Si_{13}B_{12}$	Rib.	768	786	-	1300	−33.1	-	10.1	-	-	[125]
$(Fe_{1/4}Co_{1/4}Ni_{1/4}V_{1/4})_{68}B_{32}$	Rib.	788	840	-	-	-	-	-	-	-	[203]
$[Fe_{1/4}Co_{1/4}Ni_{1/4}(Si_{0.3}B_{0.7})_{1/4}]_{99}Al_1$	Rib.	732	766	-	-	-	-	-	-	-	[203]
$[Fe_{1/4}Co_{1/4}Ni_{1/4}(Si_{0.3}B_{0.7})_{1/4}]_{98}Al_2$	Rib.	728	763	-	-	-	-	-	-	-	[203]
$[Fe_{1/4}Co_{1/4}Ni_{1/4}(Si_{0.3}B_{0.7})_{1/4}]_{97}Al_3$	Rib.	727	762	-	-	-	-	-	-	-	[203]
$[Fe_{1/4}Co_{1/4}Ni_{1/4}(Si_{0.3}B_{0.7})_{1/4}]_{95}Al_5$	Rib.	722	754	-	-	-	-	-	-	-	[203]
$[Fe_{1/4}Co_{1/4}Ni_{1/4}(Si_{0.3}B_{0.7})_{1/4}]_{92}Al_8$	Rib.	718	737	-	-	-	-	-	-	-	[203]
$Co_{28}Fe_{28}Ni_{19}Si_{13}B_8Cu_1Nb_1Mo_2$	Rib.	691	730	-	-	-	-	-	-	-	[204]
$Co_{27.5}Cr_{27.5}Mo_{26.5}Nb_{3.5}B_{15}$	Rib.	1036	1097	1605	1657	-	-	-	-	-	[205]
$Co_{26.5}Cr_{26.5}Mo_{26.5}Nb_{5.5}B_{15}$	Rib.	1048	1115	1602	1662	-	-	-	-	-	[205]
$Co_{26}Cr_{26}Mo_{26}Nb_7B_{15}$	Rib.	1058	1124	1593	1658	-	-	-	-	-	[205]
$Co_{25.5}Cr_{26.5}Mo_{25.5}Nb_{5.5}B_{17}$	Rib.	1036	1103	1583	1657	-	-	-	-	-	[205]
$Co_{24.5}Cr_{26.5}Mo_{26.5}Nb_{7.5}B_{15}$	Rib.	1029	1132	1594	1665	-	-	-	-	-	[205]
$(Al_{1/4}Ni_{1/4}Zr_{1/4}Co_{1/4})_{84}Y_{16}$	Rib.	-	742	-	-	−41.9	13.3	14.2	-	-	[206]
$(Al_{1/4}Ni_{1/4}Zr_{1/4}Co_{1/4})_{82}Y_{18}$	Rib.	-	730.5	-	-	−41.5	13.4	14.4	-	-	[206]

Continued table

Composition	D_c/ mm	T_g/ K	T_x/ K	T_m/ K	T_l/ K	ΔH_{mix}/ J·mol^{-1}	ΔS_{mix}/ J·(mol·K)$^{-1}$	δ/%	T_{rg}	γ_m	Ref.
$(Al_{1/4}Ni_{1/4}Zr_{1/4}Co_{1/4})_{80}Y_{20}$	Rib.	-	723	-	-	−41.1	13.4	14.7	-	-	[206]
$(Al_{1/4}Ni_{1/4}Zr_{1/4}Co_{1/4})_{78}Y_{22}$	Rib.	682	714	-	-	−40.7	13.4	14.8	-	-	[206]
$(Al_{1/4}Ni_{1/4}Zr_{1/4}Co_{1/4})_{76}Y_{24}$	Rib.	677	707	-	-	−40.2	13.3	15.0	-	-	[206]
$(Al_{1/4}Ni_{1/4}Zr_{1/4}Co_{1/4})_{74}Y_{26}$	Rib.	665	703	-	-	−39.7	13.3	15.1	-	-	[206]
$(Al_{1/4}Ni_{1/4}Zr_{1/4}Co_{1/4})_{72}Y_{28}$	Rib.	661	697	-	-	−39.2	13.2	15.2	-	-	[206]
$(ZrTiHfNi)_{95}Nb_5$	Rib.	694	783	994	1040	-	13.4	-	-	-	[87]
$(ZrTiHfNi)_{90}Nb_{10}$	Rib.	695	804	-	-	-	-	-	-	-	[87]
$(ZrTiHfNi)_{85}Nb_{15}$	Rib.	697	828	-	-	-	-	-	-	-	[87]
$(ZrTiHfNi)_{80}Nb_{20}$	Rib.	697	837	-	-	-	-	-	-	-	[87]
$Gd_{25}Tb_{25}Co_{25}Al_{25}$	Mic.	-	-	-	-	−35.5	11.6	15.0	-	-	[207]
$Gd_{36}Tb_{20}Co_{20}Al_{24}$	Mic.	-	-	-	-	−34.6	11.3	14.3	-	-	[207]
$Dy_{36}Tb_{20}Co_{20}Al_{24}$	Mic.	-	-	-	-	−34.6	11.3	14.4	-	-	[208]
$Ho_{36}Tb_{20}Co_{20}Al_{24}$	Mic.			-	-	−34.3	11.3	13.8	-	-	[208]
$Gd_{25}Dy_{25}Co_{25}Al_{25}$	Mic.	623	656	-	1505	−35.3	11.5	14.8	-	-	[208]
$Ho_{20}Gd_{20}Dy_{20}Co_{20}Al_{20}$	Mic.	587	616	-	1484	−32.2	13.4	13.9	-	-	[208]
$Tb_{20}Gd_{20}Dy_{20}Co_{20}Al_{20}$	Mic.	580	618	-	1482	−32.5	13.4	14.0	-	-	[208]

Table S2 Yield strength (σ_y), fracture strength (σ_f), and plasticity (ε_p) of HEMGs at room temperature

Composition	σ_y/MPa	σ_f/MPa	ε_p/%	Ref.
$Ti_{20}Zr_{20}Hf_{20}Cu_{20}Ni_{20}$	-	1920	2	[198]
$Ti_{20}Zr_{20}Hf_{20}Be_{20}Cu_{20}$	1889	1995	2.3±0.4	[16]
$Ti_{16.7}Zr_{16.7}Hf_{16.7}Be_{16.7}Cu_{16.7}Ni_{16.7}$	2019	2101	1.5±0.4	[84]
$Ti_{20}Zr_{20}Hf_{20}Be_{20}Cu_{17.5}Ni_{2.5}$	1943	2001	0.7±0.3	[38]
$Ti_{20}Zr_{20}Hf_{20}Be_{20}Cu_{12.5}Ni_{7.5}$	1992	2012	0.6±0.4	[38]
$Ti_{20}Zr_{20}Hf_{20}Be_{20}Cu_{10}Ni_{10}$	2005	2047	1.6±0.3	[38]
$Ti_{20}Zr_{20}Hf_{20}Be_{20}Cu_{7.5}Ni_{12.5}$	2067	2124	3.4±1.1	[38]
$Ti_{20}Zr_{20}Hf_{20}Be_{20}Cu_5Ni_{15}$	2088	2143	1.7±0.8	[38]
$Ti_{20}Zr_{20}Hf_{20}Be_{20}Cu_{2.5}Ni_{17.5}$	2094	2226	2.7±1.0	[38]
$(Ti_{37.31}Zr_{22.75}Be_{26.39}Al_{4.55}Cu_9)_{94}Ni_6$	2120	2265	4.3	[40]
$(Ti_{37.31}Zr_{22.75}Be_{26.39}Al_{4.55}Cu_9)_{94}Co_6$	2055	2180	5.5	[40]
$(Ti_{41}Zr_{25}Be_{29}Al_5)_{89}Cu_{5.5}Ni_{5.5}$	1925	2078	6.2	[40]
$Ti_{30}Zr_{30}Be_{20}Al_5Cu_{7.5}Ni_{7.5}$	1920	2159	7.7	[40]
$Ti_{30}Zr_{30}Be_{20}Al_5Cu_5Ni_5Co_5$	1860	1948	6.0	[40]
$Zr_{31}Ti_{27}Be_{26}Cu_{10}Fe_6$	1707	1813	0.4	[26]
$Zr_{31}Ti_{27}Be_{26}Cu_{10}Al_6$	1808	1943	2.4	[26]
$Zr_{31}Ti_{27}Be_{26}Cu_{10}Ag_6$	1717	1854	3.8	[26]
$Zr_{31}Ti_{27}Be_{26}Cu_{10}Ni_6$	1684	1896	2.8	[26]

Continued table

Composition	σ_y/MPa	σ_f/MPa	ε_p/%	Ref.
$Zr_{31}Ti_{27}Be_{26}Cu_{10}Cr_6$	1842	2003	1.6	[26]
$Zr_{31}Ti_{27}Be_{26}Cu_{10}V_6$	1731	1911	4	[26]
$Zr_{28}Ti_{24}Be_{23}Cu_9Ni_{10}Fe_6$	1911	2119	1.1	[26]
$Zr_{28}Ti_{24}Be_{23}Cu_9Ni_{10}Al_6$	1754	2014	1.6	[26]
$Zr_{33}Hf_8Ti_6Cu_{32}Ni_{10}Co_5Al_6$	-	2250	16.8	[141]
$Hf_{28}Be_{18}Ti_{17}Zr_{17}Cu_{7.5}Ni_{12.5}$	2021±13.01	2035±38.35	1±0.07	[185]
$Fe_{25}Co_{25}Ni_{25}(B_{0.6}Si_{0.4})_{25}$	-	3239	3.1	[143]
$Fe_{25}Co_{25}Ni_{25}(B_{0.7}Si_{0.3})_{25}$	-	3624	1.7	[143]
$Fe_{25}Co_{25}Ni_{25}(P_{0.5}C_{0.3}B_{0.2})_{25}$	-	2850	1.2	[195]
$Fe_{25}Co_{25}Ni_{25}(P_{0.3}C_{0.3}B_{0.4})_{25}$	-	3210	0.3	[195]
$(Fe_{1/3}Co_{1/3}Ni_{1/3})_{80}(P_{1/2}B_{1/2})_{20}$	2580	3000	4	[191]
$Fe_{25}Co_{25}Ni_{25}(P_{0.5}C_{0.1}B_{0.2}Si_{0.2})_{25}$	-	3076	1.9	[209]
$(Fe_{1/3}Co_{1/3}Ni_{1/3})_{77.5}Cr_{2.5}(P_{1/2}B_{1/2})_{20}$	3050	-	11.2	[30]
$Fe_{0.25}Co_{0.25}Ni_{0.25}(Si_{0.3}B_{0.7})_{0.25}$	3300	-	0.8	[42]
$[Fe_{0.25}Co_{0.25}Ni_{0.25}(Si_{0.3}B_{0.7})_{0.25}]_{99.7}Cu_{0.3}$	3489	-	4.7	[42]
$[Fe_{0.25}Co_{0.25}Ni_{0.25}(Si_{0.3}B_{0.7})_{0.25}]_{99.4}Cu_{0.6}$	3515	-	3.1	[42]
$Fe_{20}Co_{20}Ni_{20}Cr_5Mo_{15}P_{10}B_{10}$	3124	-	0	[142]

References

1 Ye Y F, Wang Q, Lu J *et al. Materials Today*[J], 2016, 19(6): 349

2 George E P, Raabe D, Ritchie R O. *Nature Reviews Materials*[J], 2019, 4(8): 515

3 Zhang Y, Zuo T T, Tang Z *et al. Progress in Materials Science*[J], 2014, 61: 1

4 Miracle D B, Senkov O N. *Acta Materialia*[J], 2017, 122: 448

5 Miracle D, Miller J, Senkov O *et al. Entropy*[J], 2014, 16(1): 494

6 Lu C Y, Niu L L, Chen N J *et al. Nature Communications*[J], 2016, 7: 13564

7 Senkov O N, Wilks G B, Scott J M *et al. Intermetallics*[J], 2011, 19(5): 698

8 Bernd G, Anton H, Dhiraj C *et al. Science*[J], 2014, 345(6201): 1153

9 Kiran K N A P, Li C, Leonard K J *et al. Acta Materialia*[J], 2016, 113: 230

10 El-Atwani O, Li N, Li M *et al. Science Advances*[J], 2016, 5(3): 2002

11 Yao Y G, Huang Z N, Xie P F *et al. Science*[J], 2018, 359(6383): 1489

12 Batchelor T A A, Pedersen J K, Winther S H *et al. Joule*[J], 2019, 3(3): 834

13 Xie P F, Yao Y G, Huang Z N *et al. Nature Communications*[J], 2019, 10(4011): 11848

14 Li H D, Han Y, Zhao H *et al. Nature Communications*[J], 2020, 11(5437): 19277

15 Takeuchi A, Chen N, Wada T *et al. Intermetallics*[J], 2011, 19(10): 1546

16 Zhao S F, Yang G N, Ding H Y *et al. Intermetallics*[J], 2015, 61: 47

17 Kui H W, Greer A L, Turnbull D *et al. Applied Physics Letters*[J], 1984, 45(6): 615

18 Peker A, Johnson W L. *Applied Physics Letters*[J], 1993, 63(17): 2342

19 Wang W H, Zhao R, Han R *et al. Materials Futures*[J], 2025, 4(3): 033001

20 Yang M, Liu X J, Wu Y *et al. Materials Research Letters*[J], 2018, 6(9): 495

21 Li Y H, Wang S W, Wang X W *et al. Journal of Materials Science & Technology*[J], 2020, 43: 32

22 Chong K, Gao Y, Zhang Z *et al. Corrosion Science*[J], 2023, 213: 110979

23 Zhang S, Zhang Z, Chen C *et al. Journal of Non-Crystalline Solids*[J], 2023, 601: 122049

24 Tsai K Y, Tsai M H, Yeh J W. *Acta Materialia*[J], 2013, 61(13): 4887

25 Yang K, Fan X H, Li B *et al. Journal of Thermal Analysis and Calorimetry*[J], 2018, 132(2): 979

26 Bizhanova G, Li F W, Ma Y F *et al. Journal of Alloys and*

Compounds[J], 2019, 779: 474
27 Li X, Yang K, Li B *et al. Thermochimica Acta*[J], 2023, 724: 179497
28 Xu T, Yao J S, Zhuo L C *et al. Metals*[J], 2023, 13(9): 1624
29 Wang Y, Zhang K, Feng Y H *et al. Journal of Nuclear Materials*[J], 2019, 527: 151785
30 Li M C, Guan H M, Yang S *et al. Materials Science and Engineering A*[J], 2021, 805: 140542
31 Zhou Q, Du Y, Han W C *et al. Materials & Design*[J], 2020, 189: 108500
32 Zhou Q, Du Y, Han W C *et al. Scripta Materialia*[J], 2019, 164: 121
33 Fang Q H, Yi M, Li J *et al. Applied Surface Science*[J], 2018, 443: 122
34 Zhao S F, Wang H B, Gu J L *et al. Journal of Alloys and Compounds*[J], 2018, 742: 312
35 Yeh J W, Chen S K, Lin S J *et al. Advanced Engineering Materials*[J], 2004, 6(5): 299
36 Klement W, Willens R, Duwez P. *Nature*[J], 1960, 187: 869
37 Gao X Q, Zhao K, Ke H B *et al. Journal of Non-Crystalline Solids*[J], 2011, 357(21): 3557
38 Zhao S F, Shao Y, Liu X *et al. Materials & Design*[J], 2015, 87: 625
39 Calin M, Vishnu J, Thirathipviwat P *et al. Materials Science and Engineering C*[J], 2021, 121: 111733
40 Zhong X Z, Zhang Q M, Ma M Z *et al. Journal of Materials Research and Technology*[J], 2023, 23: 5939
41 Zhu Q Y, Li R, Li Z Z *et al. Journal of Materials Research and Technology*[J], 2023, 25: 2275
42 Fan X, Xie L, Li Q *et al. Acta Metallurgica Sinica* (*English Letters*)[J], 2023, 36(3): 417
43 Xu Y Q, Li Y H, Zhu Z W *et al. Journal of Non-Crystalline Solids*[J], 2018, 487: 60
44 Panahi S L, Garcia-Ramón M, Pineda E *et al. Journal of Non-Crystalline Solids*[J], 2020, 547: 120301
45 Zhang H, Chen C, Fan Y Z *et al. Journal of Magnetism and Magnetic Materials*[J], 2020, 509: 166875
46 Kim J, Oh H S, Kim J *et al. Acta Materialia*[J], 2018, 155: 350
47 Shao L L, Wang Q Q, Xue L *et al. Journal of Materials Research and Technology*[J], 2021, 11: 378
48 Li J, Xue L, Yang W M *et al. Intermetallics*[J], 2018, 96: 90
49 Pang C M, Chen L, Xu H *et al. Journal of Alloys and Compounds*[J], 2020, 827: 154101
50 Pan J, Wang Y X, Li Y. *Acta Materialia*[J], 2017, 136: 126
51 Tian L, Cheng Y Q, Shan Z W *et al. Nature Communications*[J], 2012, 3: 609
52 Greer J R, Jang D. *Nature Materials*[J], 2010, 9: 215
53 Hofmann D C, Suh J Y, Wiest A *et al. Nature*[J], 2008, 451: 1085
54 Inoue A, Shen B, Koshiba H *et al. Nature Materials*[J], 2003, 2: 661
55 Kumar G, Ohkubo T, Hono K. *Journal of Materials Research*[J], 2011, 24(7): 2353
56 Johnson L F P, Fullerton J, Bluestone J *et al*. *Human Resources for Health*[J], 2013, 11: 42
57 Sun B A, Wang W H. *Progress in Materials Science*[J], 2015, 74: 211
58 Suryanarayana C, Inoue A. *International Materials Reviews*[J], 2013, 58(3): 131
59 Zberg B, Uggowitzer P J, Löffler J F. *Nature Materials*[J], 2009, 8(11): 887
60 Wang W H. *Advanced Materials*[J], 2009, 21(45): 4524
61 Xia L, Fang S S, Wang Q. *Applied Physics Letters*[J], 2006, 88: 171905
62 Ito K. *Nature*[J], 1999, 398: 492
63 Zhang Y, Zhou Y J, Hui X D *et al. Science in China Series G: Physics, Mechanics and Astronomy*[J], 2008, 51(4): 427
64 Yang L, Guo G Q, Chen L Y *et al. Physical Review Letters*[J], 2012, 109: 10
65 Chen H S. *Reports on Progress in Physics*[J], 1980, 43(4): 353
66 Wang W H, Dong C, Shek C H. *Materials Science and Engineering R: Reports*[J], 2004, 44(2–3): 45
67 Inoue A. *Materials Transactions, JIM*[J], 1995, 36: 866
68 Inoue A. *Acta Materialia*[J], 2000, 40: 279
69 Lu Z P, Liu C T. *Acta Materialia*[J], 2002, 50: 3501
70 Greer A L. *Nature*[J], 1993, 366: 303
71 Inoue A, Masumoto T. *Materials Transactions, JIM*[J], 1990, 31: 425
72 Ma L W, Zhang T, Inoue A. *Materials Transactions, JIM*[J], 2002, 43: 277
73 Wang W H. *JOM*[J], 2014, 66(10): 2067
74 Qiao J C, Wang Q, Pelletier J M *et al. Progress in Materials Science*[J], 2019, 104: 250
75 Chen Y, Dai Z W, Jiang J Z. *Journal of Alloys and Compounds*[J], 2021, 866: 158852
76 Luan H W, Li K R, Shi L X *et al. Journal of Materials Science & Technology*[J], 2023, 161: 50
77 Konchakov R A, Makarov A S, Afonin G V *et al. JETP Letters*[J], 2024, 119(6): 458
78 Yang X, Zhang Y. *Materials Chemistry and Physics*[J], 2012, 132(2–3): 233
79 Makarov A S, Konchakov R A, Afonin G V *et al. JETP Letters*[J], 2024, 120(10): 759
80 Wang X D, Wei S F, Qiu K K *et al. Journal of Alloys and Compounds*[J], 2024, 976: 172947
81 Ding J, Inoue A, Han Y *et al. Journal of Alloys and Compounds*[J], 2017, 696: 345
82 Wang X Y, Dai W L, Zhang M *et al. Journal of Materials Science & Technology*[J], 2018, 34(11): 2006
83 Jin F, Yuan C C, Pang C M *et al. Materials & Design*[J], 2024, 238: 112653
84 Ding H Y, Shao Y, Gong P *et al. Materials Letters*[J], 2014, 125: 151

85 Yang Q, Yang X M, Zhang T *et al. Acta Materialia*[J], 2024, 266: 119701

86 Wang X Y, Maresca F, Cao P H. *Acta Materialia*[J], 2022, 234: 118022

87 Chong K, Gao Y, Zhang Z B *et al. Journal of Materials Research and Technology*[J], 2025, 36: 699

88 Chong K, Gao Y, Zhang Z B *et al. Journal of Non-Crystalline Solids*[J], 2025, 658: 123536

89 Bazlov A, Ubyivovk E, Zanaeva E *et al. Intermetallics*[J], 2025, 184: 108850

90 Li X, Shan G C, Shek C H. *Journal of Materials Science & Technology*[J], 2022, 103: 113

91 Ding H Y, Zhang Q, Yao K F. *Materials*[J], 2024, 17: 453

92 Wang F, Inoue A, Kong F L *et al. Journal of Alloys and Compounds*[J], 2018, 732: 637

93 Makarov A S. *JETP Letters*[J], 2023, 118(3): 182

94 Jiang J, Lu Z, Shen J *et al. Nature Communications*[J], 2021, 12: 3843

95 Li T Q, Zong H X, Zhao F H *et al. Acta Materialia*[J], 2023, 257: 119196

96 Li T Q, Wang Y D. *Scripta Materialia*[J], 2024, 252: 116255

97 Luan H W, Zhang X, Ding H Y *et al. Nature Communications*[J], 2022, 13: 2183

98 Konchakov R A, Makarov A S, Afonin G V *et al. Journal of Non-Crystalline Solids*[J], 2023, 619: 122555

99 Shen J, Lu Z, Wang J Q *et al. The Journal of Physical Chemistry Letters*[J], 2020, 11(16): 6718

100 Lan S, Ren Y, Wei X Y *et al. Nature Communications*[J], 2017, 8: 14679

101 Cao Y H, Yang M, Du Q *et al. Nature Communications*[J], 2024, 15: 6702

102 Zhang J X, Chen M H, Lin D M *et al. Journal of Physics: Condensed Matter*[J], 1989, 1(48): 19717

103 Egami T, Poon S J, Zhang Z *et al. Physical Review B*[J], 2007, 76(2): 024203

104 Patel A T, Pratap A. *Journal of Thermal Analysis and Calorimetry*[J], 2012, 110(2): 567

105 Liu C, Pineda E, Crespo D. *Metals*[J], 2015, 5(2): 1073

106 Egami T. *Journal of Alloys and Compounds*[J], 2011, 509: S82

107 Dmowski W, Fan C, Morrison M *et al. Materials Science and Engineering A*[J], 2007, 471(1–2): 125

108 Yu H B, Shen X, Wang Z *et al. Physical Review Letters*[J], 2012, 108(1): 015504

109 Yu H B, Wang W H, Samwer K. *Materials Today*[J], 2013, 16(5): 183

110 Wang Q, Zhang S T, Yang Y *et al. Nature Communications*[J], 2015, 6: 7876

111 Küchemann S, Maaß R. *Scripta Materialia*[J], 2017, 137: 5

112 Hiorns J E, Jensen O E, Brook B S. *Journal of Applied Physiology*[J], 2016, 121(1): 233

113 Wang W H. *Progress in Materials Science*[J], 2019, 106: 100561

114 Duan Y J, Nabahat M, Tong Y *et al. Physical Review Letters*[J], 2024, 132: 5

115 Duan Y J, Zhang L T, Qiao J C *et al. Physical Review Letters*[J], 2022, 129: 17

116 Tsyplakov A, Mitrofanov Y P, Makarov A *et al. Journal of Applied Physics*[J], 2014, 116: 12

117 Picard M A, Solana P, Urchueguía J F. *Journal of Sound and Vibration*[J], 1998, 216(3): 495

118 Liao D, Estévez-Salmerón L, Tlsty T D. *Physical Biology*[J], 2012, 9(6): 065005

119 Chen C J, Xu R, Yin B J *et al. Intermetallics*[J], 2023, 157: 107887

120 Wang F, Inoue A, Kong F L *et al. Acta Materialia*[J], 2019, 170: 50

121 Wang G T, Yang Y Z. *Journal of Materials Science: Materials in Electronics*[J], 2025, 36: 1092

122 Ding H Y, Yao K F. *Journal of Non-Crystalline Solids*[J], 2013, 364: 9

123 Gong P, Zhao S F, Ding H Y *et al. Journal of Materials Research*[J], 2015, 30(18): 2772

124 Gong P, Wang S B, Li F W *et al. Metallurgical and Materials Transactions A*[J], 2018, 49(7): 2918

125 Liu J H, Liu R R, Zhang X L *et al. Intermetallics*[J], 2024, 164: 108086

126 Bazlov A, Ubyivovk E, Tabachkova N *et al. Scripta Materialia*[J], 2025, 265: 116725

127 Wu J L, Li W H, Pan Y *et al. Materials & Design*[J], 2016, 89: 1130

128 Hammid A T, Razavinejad S. *Advances in Materials Science and Engineering*[J], 2022, 10: 5168629

129 Bykov V A, Kovalenko D A, Sterkhov E V *et al. Chimica Techno Acta*[J], 2023, 10(2): 7

130 Zhao R, Chen C J, Zhang F *et al. Journal of Alloys and Compounds*[J], 2025, 1022: 179829

131 Trexler M M, Thadhani N N. *Progress in Materials Science*[J], 2010, 55: 8

132 Egami T, Iwashita T, Dmowski W. *Metals*[J], 2013, 3(1): 77

133 Schuh C, Hufnagel T, Ramamurty U. *Acta Materialia*[J], 2007, 55(12): 4067

134 Xu J, Ramamurty U, Ma E. *JOM*[J], 2010, 62(4): 10

135 Gong P, Yin G, Jamili-Shirvan Z *et al. Materials Science and Engineering A*[J], 2020, 797: 140078

136 Yan X, Zhang C, Li Y S *et al. Journal of Materials Science & Technology*[J], 2022, 106: 257

137 Cheng Y Q, Sheng H W, Ma E. *Physical Review B*[J], 2008, 78: 1

138 Scudino S, Surreddi K B, Wang G *et al. Scripta Materialia*[J], 2010, 62(10): 750

139 Zhao Z, Liu J. *Journal of Alloys and Compounds*[J], 2023, 946: 169424

140 Du Q, Liu X J, Fan H Y *et al. Materials Today*[J], 2019, 34: 66

141 Jalali A, Malekan M, Park E S *et al. Journal of Alloys and Compounds*[J], 2021, 892: 162220

142 Zhang R B, Zhang C W, Xie L *et al. Journal of Non-Crystalline Solids*[J], 2022, 593: 121754

143 Qi T, Li Y, Takeuchi A *et al. Intermetallics*[J], 2015, 66: 8

144 Divinski S V, Pokoev A V, Esakkiraja N *et al. Diffusion Foundations*[J], 2018, 17: 69

145 Zhao K, Xia X X, Bai H Y *et al. Applied Physics Letters*[J], 2011, 98: 14

146 Sun B A, Hu Y C, Wang D P *et al. Acta Materialia*[J], 2016, 121: 266

147 Wang S, Ye Y F, Wang Q *et al. Scripta Materialia*[J], 2017, 130: 283

148 Qin F, Dai K Q, Chen S H *et al. Materials Today Communications*[J], 2024, 38: 107932

149 Afonin G V, Qiao J C, Makarov A S *et al. Applied Physics Letters*[J], 2024, 124: 15

150 Argibay N, Johnson D D, Chandross M *et al. Acta Materialia*[J], 2025, 290: 120990

151 Li T Q, Pang X Y, Wang Y D *et al. Acta Materialia*[J], 2025, 292: 121078

152 Zhang Y, Zhou Y, Wang L M *et al. Acta Materialia*[J], 2023, 255: 119031

153 Liu X, Di S Y, Liu L C *et al. Materials Research Letters*[J], 2025, 13(8): 810

154 Gao Y W, Wang W, Song Y *et al. Journal of Alloys and Compounds*[J], 2025, 1041: 183691

155 Song J Q, Zhu W Q, Wei X D. *International Journal of Mechanical Sciences*[J], 2021, 204: 106570

156 Geng C, Huang B, Sun K *et al. Materials Science and Engineering A*[J], 2022, 858: 144197

157 Liu C Y, Wang Y C, Wang Y C *et al. Acta Materialia*[J], 2023, 259: 119281

158 Hong Y R, Wang H, Li X *et al. Matter*[J], 2023, 6(4): 1160

159 Ma Z C, Lu F Z, Ma X X *et al. Applied Surface Science*[J], 2020, 506: 145044

160 Martin I, Ohkubo T, Ohnuma M *et al. Acta Materialia*[J], 2004, 52(15): 4427

161 Löffler J F, Johnson W L. *Applied Physics Letters*[J], 2000, 76(23): 3394

162 González S, Wurster S, Garay-Reyes C G *et al. Journal of Alloys and Compounds*[J], 2025, 1024: 180196

163 Wang Y Y, Zhu Z W, Wang A M *et al. Journal of Non-Crystalline Solids*[J], 2022, 577: 121323

164 Odbadrakh K, Enkhtor L, Amartaivan T *et al. Journal of Applied Physics*[J], 2019, 126(9): 095104

165 Chen C, Wong K, Krishnan R P *et al. Journal of Materials Science & Technology*[J], 2019, 35(1): 44

166 Chen C, Wong K, Krishnan R P *et al. Journal of Physics D: Applied Physics*[J], 2018, 51(14): 145301

167 Ye Y F, Liu X D, Wang S *et al. Intermetallics*[J], 2016, 78: 30

168 Zhang X, Luan H, Lou H *et al. Materials Today Physics*[J], 2022, 27: 100799

169 Zhang H Z, Sun H G, Pan S P *et al. Journal of Non-Crystalline Solids*[J], 2021, 553: 120501

170 Liu S N, Wang L F, Ge J C *et al. Acta Materialia*[J], 2020, 200: 42

171 Mattern N, Stoica M, Vaughan G *et al. Acta Materialia*[J], 2012, 60(2): 517

172 Yavari A R, Moulec A L, Inoue A *et al. Acta Materialia*[J], 2005, 53(6): 1611

173 Castellero A, Moser B, Uhlenhaut D I *et al. Acta Materialia*[J], 2008, 56(15): 3777

174 Georgarakis K, Louzguine-Luzgin D V, Antonowicz J *et al. Acta Materialia*[J], 2011, 59(2): 708

175 Lin H J, He M, Pan S P *et al. Acta Materialia*[J], 2016, 120: 68

176 Xing G H, Hao Q, Zhu F *et al. Science China Physics, Mechanics & Astronomy*[J], 2024, 67(5): 256111

177 Wang T, Zhou Y L, Zhang L S. *Journal of Non-Crystalline Solids*[J], 2023, 603: 122115

178 Gu J L, Luan H W, Zhao S F *et al. Materials Science and Engineering A*[J], 2020, 786: 139417

179 Wang X, Shao Y, Gong P *et al. Journal of Alloys and Compounds*[J], 2013, 575: 449

180 Tsai M H, Yeh J W. *Materials Research Letters*[J], 2014, 2(3): 107

181 Wada T, Jiang J, Yubuta K *et al. Materialia*[J], 2019, 7: 100372

182 Zhao J, Li B, Huang W *et al. Transactions of the Indian Institute of Metals*[J], 2023, 76(5): 1165

183 Chen C, Pang S, Cheng Y *et al. Journal of Non-Crystalline Solids*[J], 2015, 410: 39

184 Zong H, Geng C, Kang C *et al. Results in Physics*[J], 2018, 8: 253

185 Li X, Fan X, Li B *et al. Journal of Materials Research and Technology*[J], 2022, 21: 1331

186 Yang K, Li B, Fan X H *et al. Journal of Thermal Analysis and Calorimetry*[J], 2023, 148(3): 689

187 Bi Q, Liu J, Li J *et al. Journal of Alloys and Compounds*[J], 2025, 1016: 178858

188 Ye J, Chen Y, Bai X *et al. Materials Science and Engineering A*[J], 2025, 942: 148691

189 Li H F, Xie X H, Zhao K *et al. Acta Biomaterialia*[J], 2013, 9(10): 8561

190 Ding H Y, Luan H W, Bu H T *et al. Materials*[J], 2022, 15(5): 1669

191 Li C Z, Li Q, Li M C *et al. Journal of Alloys and Compounds*[J], 2019, 791: 947

192 Huo Y L, Zhang W, Zheng C *et al. Journal of Non-Crystalline Solids*[J], 2025, 665: 123628

193 Wu K N, Liu C, Li Q *et al. Journal of Magnetism and Magnetic Materials*[J], 2019, 489: 165404

194 Takeuchi A, Wang J, Chen N *et al. Materials Transactions*[J], 2013, 54(5): 776
195 Li Y, Zhang W, Qi T *et al. Journal of Alloys and Compounds*[J], 2017, 693: 25
196 Huo J T, Huo L S, Li J W *et al. Journal of Applied Physics*[J], 2015, 117(7): 073902
197 Kim K B, Warren P J, Cantor B. *Materials Science and Engineering A*[J], 2004, 375–377: 317
198 Tong C J, Chen Y L, Chen S K *et al. Metallurgical and Materials Transactions A*[J], 2005, 36: 881
199 Wu J L, Zhou Z Y, Yang H *et al. Journal of Alloys and Compounds*[J], 2020, 827: 154298
200 Luo L, Shen H X, Bao Y *et al. Journal of Magnetism and Magnetic Materials*[J], 2020, 507: 166856
201 Zhang Y, Zhu J, Li S *et al. Journal of Materials Science & Technology*[J], 2022, 102: 66
202 Zhang X Y, Yang Y Y, Liu Y J *et al. Advanced Materials*[J], 2023, 35(38): 2303499
203 Zhang S Y, Shi M X, Zhang Z B *et al. Materials Letters*[J], 2024, 362: 136216
204 Dai Z K, Zhou X, Wu Y *et al. Journal of Magnetism and Magnetic Materials*[J], 2024, 603: 172234
205 Zhou Y, Wang T. *Journal of Materials Research and Technology*[J], 2024, 30: 256
206 Zhang Z B, Zhang S Y, Jing Z Y *et al. Intermetallics*[J], 2024, 165: 108164
207 Yin H, Wang J Q, Huang Y *et al. Journal of Materials Science & Technology*[J], 2023, 149: 167
208 Wei S J, Dahlström A, Shen H X *et al. Journal of Alloys and Compounds*[J], 2024, 1006: 176308
209 Zhang Z, Song K, Li R *et al. Materials*[J], 2019, 12(4): 590

高熵金属玻璃：近期研究进展

徐　舟，崔佳音，何　畅，古京达，王　庆
(上海大学 材料科学与工程学院 核电关键材料全国重点实验室，上海 200444)

摘　要：近年来，高熵金属玻璃因其高构型熵，往往呈现出独特的结构特征与性能，包含迟滞扩散效应、结构非均匀性、更高的玻璃形成能力、热稳定性或力学稳定性等，因而受到越来越多的研究关注。尽管与传统金属玻璃一样，高熵金属玻璃原子结构缺乏长程周期性，但是其高熵特性却会引起结构演化的额外复杂性，如导致解耦玻璃转变、潜在的玻璃-玻璃转变以及在再加热过程中的连续多晶型转变的出现。由此，高熵金属玻璃的原子重排和相互作用、化学/拓扑非均匀性具备可调控性，进而使其具有很强的结构与功能应用潜力。尽管已有若干关于高熵金属玻璃的综述报道，鉴于该领域研究的快速推进，本文对高熵金属玻璃合金体系的最新进展做出进一步简要综述与讨论。首先聚焦于新开发高熵金属玻璃的玻璃形成能力；随后，将其不同寻常的结构弛豫、结晶行为及力学性能等与传统金属玻璃相比较；最后，对高熵金属玻璃的原子尺度结构与结构非均匀性特征进行综合评述，并给出总结与展望。

关键词：高熵金属玻璃；玻璃形成能力；热稳定性；力学性能；原子尺度结构

作者简介：徐　舟，女，2001年生，上海大学材料科学与工程学院核电关键材料全国重点实验室，上海 200444，E-mail：Xu_Z@shu.edu.cn